

CHALMERS



Development of a Wave Database in Coastal Areas around Sweden Using the SWAN Wave Model

Evaluation of the influence of grid resolutions and bathymetric data

Master of Science Thesis in the Master's Programme Geo and Water Engineering

SINA SAREMI

Department of Civil and Environmental Engineering
Division of Water and Environment Technology
CHALMERS UNIVERSITY OF TECHNOLOGY
Göteborg, Sweden 2010
Master's Thesis 2010:33

MASTER'S THESIS 2010:33

Development of a Wave Database in Coastal Areas around Sweden Using the SWAN Wave Model

Evaluation of the influence of grid resolutions and bathymetric data

Master of Science Thesis in the Master's Programme Geo and Water Engineering

SINA SAREMI

Department of Civil and Environmental Engineering
Division of Water and Environment Technology
CHALMERS UNIVERSITY OF TECHNOLOGY

Göteborg, Sweden 2010

Development of a Wave Database in Coastal Areas around Sweden Using the SWAN
Wave Model

Evaluation of the influence of grid resolutions and bathymetric data
Master of Science Thesis in the Master's Programme Geo and Water Engineering
SINA SAREMI

© SINA SAREMI, 2010

Examensarbete / Institutionen för bygg- och miljöteknik,
Chalmers tekniska högskola 2010:

Department of Civil and Environmental Engineering
Division of Water and Environment Technology
Chalmers University of Technology
SE-412 96 Göteborg
Sweden
Telephone: + 46 (0)31-772 1000

Cover:
Seawatch buoy located east of Huvudskär in the Baltic

Reproservice/ Department of Civil and Environmental Engineering
Göteborg, Sweden 2010

Development of a Wave Database in Coastal Areas around Sweden Using the SWAN Wave Model

Evaluation of the influence of grid resolutions and bathymetric data

Master of Science Thesis in the Master's Programme Geo and Water Engineering

SINA SAREMI

Department of Civil and Environmental Engineering

Division of Water and Environment Technology

Chalmers University of Technology

ABSTRACT

A 15 year hindcast wave database for the Baltic Sea, Kattegat and Skagerrak was developed in 2008. The phase averaged third generation spectral model SWAN (Simulating WAVes Nearshore) was used for simulating the wind-waves. The wind force used for the wave simulation was coming from the RCA model with grid resolution of 12×12 NM (nautical miles). The computational grid and bathymetric database had the resolution of 6×6 NM which was too coarse for having detailed information at the coastal areas.

In this project the mentioned database is modified by using a finer computational grid, better resolved bathymetric data (from HIROMB database) and including shallow water physics in the simulation. Atmospheric forcing and other inputs have not been modified. Applying unstructured triangular computational grids did not give any satisfactory results. The combination of better bathymetric data with the resolution of 1×1.6 NM, a finer structured computational grid with the resolution of 3×3 NM and including shallow water physics has slightly improved the results at the measurement stations compared to the previous database. The better resolution and bathymetry gives more detailed information along the coastlines. At this point, a more realistic atmospheric forcing is needed to further improve the results.

Key words: SWAN, unstructured, computational grid, spectral model, Baltic Sea, wind-waves

Contents

1	INTRODUCTION	1
1.1	Scope of Work	1
1.2	Similar projects	2
2	THEORY	3
2.1	Ocean Waves	3
2.1.1	The simple linear wave	3
2.1.2	Wave fields on the ocean	3
2.1.3	Statistical description of waves	5
2.1.4	The wave spectrum	6
2.2	Wave modelling	9
2.3	Wave generation	10
2.3.1	Resonance	11
2.3.2	Shear flow	11
2.4	Wave dissipation	13
2.4.1	Wave breaking in the surf zone	14
2.4.2	Bottom friction	15
2.4.3	White-capping	16
2.5	Nonlinear wave-wave interactions	16
2.6	Coriolis Effect	17
2.7	SWAN	18
3	METHOD	19
3.1	Nesting	19
3.2	Coordinate system and grid translation	20
3.3	Computational Grids	22
3.3.1	Unstructured grids	22
3.3.2	Structured grids	23
3.4	Physics	24
3.5	Input data	24
3.5.1	Wind	24
3.5.2	Bathymetry	24
3.5.3	Ice coverage	25
3.5.4	Boundary conditions	25
3.6	Measured data sources	25
3.7	Parallel processing	26
4	RESULTS	28

4.1	Calibration	28
4.2	Validation	32
4.3	Simulations time and data capacity	36
4.4	Comparison with previous simulation in 2008	37
5	DISCUSSION	39
5.1	Improvements to previous database	40
5.2	Recommendations for further investigation and more development	40
6	REFERENCES	41

Preface

In this study a 15 year hindcast database of wind-waves in the Baltic Sea, Skagerack and Kattegat has been developed using the SWAN Cycle III version 40.72 ABCD. It is a project at Swedish Meteorological and Hydrological Institute (SMHI). The work has been carried out from September 2009 to May 2010 at the SMHI office in Göteborg, Sweden.

The work has been made by the author under the supervision and cooperation of Walter Gyllenram at SMHI and under the supervision of Professor Lars Bergdahl at Chalmers University, who also has been the examiner. I would also like to thank all SMHI staff who always helped me with any questions.

Göteborg May 2010

Sina Saremi

Notations

$A(f,\theta)$	Resonant interaction function
a	Wave amplitude
$B(f,\theta)$	Shear flow growth function
c	Wave speed
C_d	Drag coefficient
C_f	Bottom friction coefficient
C_g	Wave group velocity
E	Total energy in the wave field
$E(f,\theta)$	Wave energy spectrum
F	Directional spectrum of the waves
f	Coriolis parameter
f	Wave frequency
f_p	Wave frequency corresponding to the peak of spectrum
g	Acceleration of gravity
\bar{H}	Average wave height
H_{max}	Maximum wave height occurring in a record
H_{rms}	Root-mean-square wave height
H_s	Significant wave height
$H_{1/n}$	The average height of the 1/n highest waves
$H_{1/3}$	Significant wave height
h	Depth
h_w	Height of the white-cap region
j	Number of wave component
K	Kernel function
k	Wave number
L	Length
L_w	Length of the white-cap region
m_n	nth-order moment of the spectrum
n	Total number of wave components
n_i	Wave action density
NM	Nautical Miles
$P(H)$	Rayleigh probability density distribution
$P(k,f)$	Spectrum of wave-induced turbulence
Q_b	Fraction of waves which are breaking
R	The Rossby number
S_{br}	Dissipation source term for surf breaking
S_{bf}	Dissipation source term for bottom friction
S_{wc}	Dissipation source term for white-capping
S_{tot}	Summation of all source terms
S_{in}	Atmospheric input source term
S_{nl}	Nonlinear wave-wave interactions source term
S_{ds}	Dissipation source term
T_{m01}	Wave period corresponding to the mean period of the spectrum
T_{m02}	Mean zero crossing wave period
T_p	Wave period corresponding to the peak of the spectrum

T_z	Mean zero down-crossing wave period
$T_{1/n}$	The average period of the 1/n highest waves
$T_{1/3}$	Significant wave period
t	Time
U	Velocity
$U(y)$	Wind velocity vertical distribution
U_5	Wind speed at 5 meters height
u	wind speed
u_b	Water velocity just above the bottom
u_*	Friction velocity
x	Coordinate in x direction
y	Coordinate in y direction
y_c	Height of critical zone in shear-flow growth mechanism
η	Recorded elevation of the water surface
η_0	Mean water elevation
γ_{ds}	Damping coefficient
θ	Wave direction
λ	Wave length
μ	Coupling coefficient
$\Pi(k, \theta)$	Wave number, frequency spectrum of atmospheric pressure
ρ_a	Air density
ρ_w	Water density
σ^2	Variance of the wave record
τ	Wind stress
τ	Water stress on bottom
ψ	Wind direction
Ω	Angular velocity of plenary rotation
ω_0	Angular frequency of the longest wave fitted to the record
Φ	Latitude
φ	phase angel of the wave component

1 Introduction

In 2008 the Swedish Meteorological and Hydrological Institute (SMHI) set up a “Hindcast wave data base of the Baltic Sea” (Broman & Kriezi 2008). The wave simulations were focused on waves in offshore areas, using the SWAN program. The data base was first intended to cover 44 years from 1960 to 2004, but the information of ice concentration before 1980 was still in process. They only completed 15 years of hindcast run (1990-2004), in order to satisfy the pressure of incoming external projects. This data base is widely used by the consultancy departments in various projects.

However, there is an increasing demand of wave data/statistics for areas close to the coast. The mentioned data base cannot provide information for the coastal areas for two reasons:

1. The computational resolution is very coarse (6×6 Nautical Miles)
2. The wave simulation only includes the physical mechanism of propagation and dissipation of waves in deep water.

The goal of this project is to develop a wave database, using the SWAN numerical model, by refining the computational grids and using better resolved bathymetric data compared to these from 2008. This would increase the data quality which is required in coastal and near shore areas. Also by comparing the results to the ones from 2008, the influence of refined computational grids and resolved bathymetric data on simulation outputs by SWAN is evaluated.

The simulation in 2008 was composed of one run with the resolution of 12×12 NM covering the North Sea and a nested run with the resolution of 6×6 NM covering Skagerack, Kattegatt and the Baltic Sea. The bathymetric data had the resolution of 6×6 NM. The new run will cover the same regions but aims at using finer grids and a more detailed bathymetry.

1.1 Scope of Work

This thesis focuses on evaluating the effect of modified computational grids, better resolved bathymetric data and including shallow water effects such as triad wave-wave interactions on the quality of the results from the SWAN program. The whole region will be simulated in a coarse computational grid (6×6 NM). A relatively small area with different refined mesh grids will be nested into the former and simulated for one year period (1990). Comparing the results from the nested runs to available measurements will lead to finding an optimum grid resolution. Then the validation will be done by running the model on the whole region for the year 1999. The results will be compared to the ones from 2008. This will give a clue of how computational and bathymetric grid refinements can influence outputs from the SWAN wave model. The most suitable computational grid resolution for developing the 15 year hindcast is determined as well.

1.2 Similar projects

There are many projects done in the field of simulating the near shore waves. For instance, Hoque et al. (2009) simulated the near shore waves in the southern Beaufort Sea, using SWAN model under its non-stationary and two-dimensional mode in a fine resolution domain nested within a coarse domain.

Barstow et al. (2009) have made a WorldWaves wave energy resource assessment from the deep ocean to the coast. The offshore data were provided by ECMWF (The European Centre for Medium-Range Weather Forecasts) which uses WAM model. These data were used as boundary conditions for SWAN model nesting coastal areas.

Wamsley (2009) in modelling the interaction of hurricanes and natural coastal features in southern Louisiana has used WAM model to simulate the offshore waves then runs a nested simulation by STWAVE model at coastal areas.

Rusu (2009) has modelled the Black Sea by the SWAN model in a wave energy assessment project using a grid with the resolution of 0.08° covering the western part of the Black Sea.

Broman and Kriezi (2008) simulated the same area as in this project with 6×6 NM computational and bathymetric grids to create a hindcast. They also evaluated the influence of quality of wind forcing data on the results from the SWAN. The better resolved wind data enhanced the simulation results significantly. Same result was obtained by Howard et al. (2009) in evaluating the impact of atmospheric model resolution on a coupled wind/wave forecast system, using CMS-Wave (formerly known as WABED).

2 Theory

2.1 Ocean Waves

2.1.1 The simple linear wave

The simplest wave motion can be represented by a sinusoidal wave. A sinusoidal wave has the smooth shape of a sine curve.

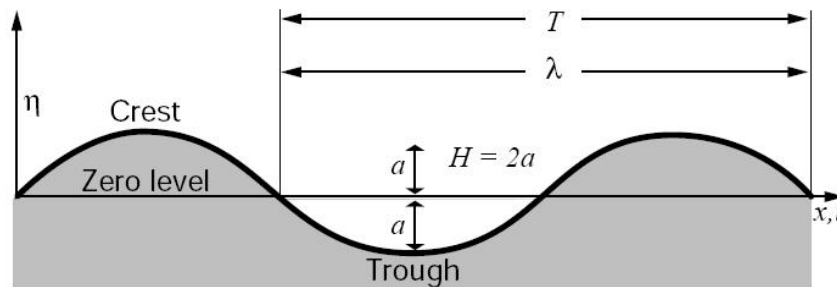


Figure 1: A simple sinusoidal wave

The wave length, λ , is the horizontal distance between two successive crests. The period, T , is the time interval between the passages of successive crests through a fix point. The amplitude, a , is the magnitude of the maximum displacement from mean sea level. The wave height, H , is the difference in surface elevation, η , between the wave crest and the previous wave trough.

2.1.2 Wave fields on the ocean

The actual sea waves do not look like the one in Figure 1. They appear with irregular shapes and constantly changing water surface, since waves are being overtaken and crossed by others. Figure 2 shows an observed pattern from an actual sea.

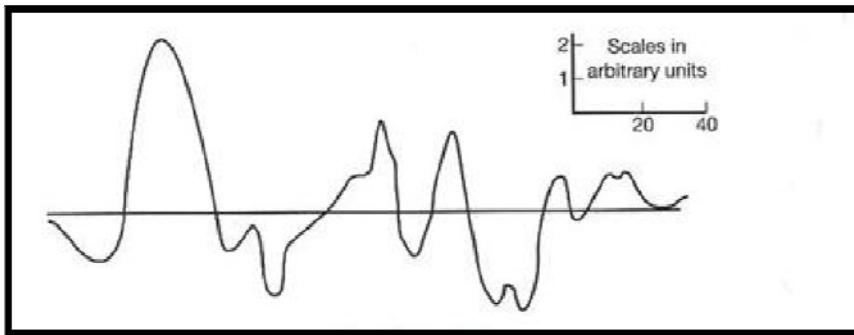


Figure 2: Sample record from the actual sea

Any observed wave pattern on the ocean can be shown to compromise a number of simple waves with different heights, periods and directions. This idea shows how an irregular pattern of waves can be considered as superposition of an infinite number of sinusoidal waves propagating independently of each other.

Observing the waves carefully in the sea, one can see how waves with similar wavelengths combine and move with each other forming groups of waves. Each individual wave travels with a speed related to its wave length. However the group as a coherent unit advances with its own velocity. This velocity is accordingly named as the group velocity, c_g . In deep water it is defined as:

$$c_g = \frac{c}{2}$$

where c is the velocity of each individual wave.

A general expression for group velocity in finite depth water is as below:

$$c_g = \frac{c}{2} \left(1 + \frac{2kh}{\sinh 2kh} \right)$$

$$k = \frac{2\pi}{\lambda}$$

where k is the wave number, h is the water depth and λ is the wave length. (WMO, 1998)

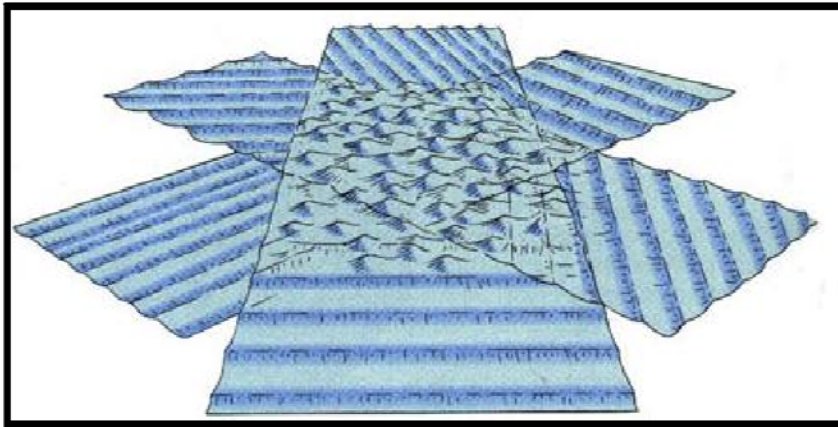


Figure 3: The sea surface obtained from the sum of many sinusoidal waves

2.1.3 Statistical description of waves

A typical wave record from a rather confusing pattern in an actual sea is shown in figure 4. Wave crests are marked by dashes and all zero down-crossings are circled. The wave period is the time between two consecutive down-crossings (or up-crossings; there is no clear convention in choosing them, as in long records it makes almost no difference). The wave height H is the vertical distance from a trough to the next crest.

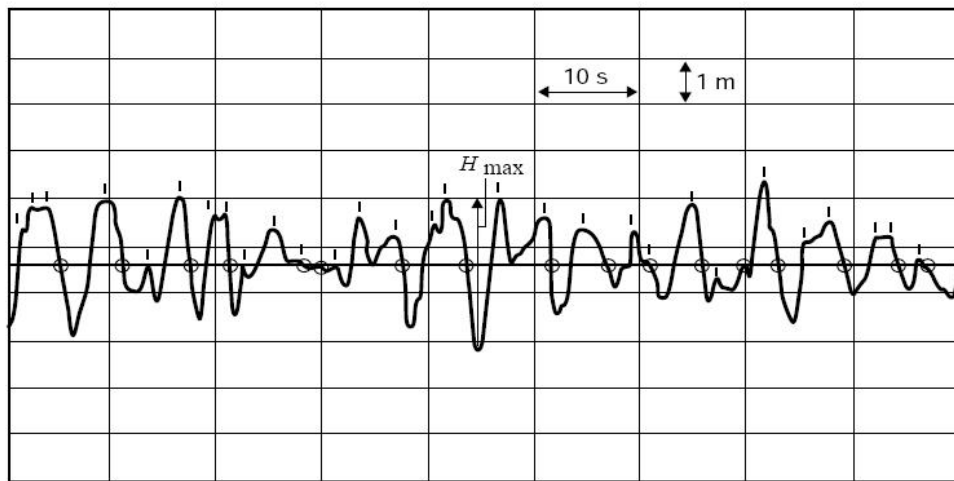


Figure 4: Sample of a wave record

A measured wave record never repeats, but if the conditions are stationary the statistical properties of the distributions of periods and heights will be the same from one record to another. Hence, the best way to describe the sea state is by the statistical parameters. The most frequently used parameters are:

- \bar{H} = Average wave height;
 - H_{\max} = Maximum wave height occurring in a record;
 - \bar{T}_z = Average zero-crossing wave period;
 - $\bar{H}_{1/n}$ = The average height of the $1/n$ highest waves;
 - $\bar{T}_{1/n}$ = The average period of the $1/n$ highest waves;
- A commonly used value for n is 3:
- $\bar{H}_{1/3}$ = Significant wave height (H_s)
 - $\bar{T}_{1/3}$ = Significant wave period

2.1.4 The wave spectrum

Sea surface with a random appearance could be regarded as the sum of many simple waves. A way to define this concept is to introduce the wave spectrum. A wave record may be decomposed by means of harmonic (or Fourier) analysis to large number of sinusoidal waves with different frequencies, amplitudes, directions and phases. Each frequency and direction describes a wave component which has an associated amplitude and phase. For a surface elevation varying in time in a single direction:

$$\eta(t) = \eta_0 + \sum_{j=1}^n a_j \sin(j\omega_0 t + \phi_j)$$

In which:

- $\eta(t)$ = recorded elevation of the water surface at time t
- η_0 = mean elevation
- ω_0 = angular frequency of the longest wave fitted to the record
- j = number of wave component
- a_j = amplitude of the j th component
- ϕ_j = phase angle of the j th component
- n = total number of components

The expected values of the squares of the amplitudes a_j are the contribution to the variance of the surface elevation η from each of the wave components ($E[\sum_j a_j^2]$). The resulting function is known as the wave-variance spectrum. Since the wave energy equals $\rho_w g H^2 / 8$ or $\rho_w g a^2 / 2$ ($H=2a$), in some literature the wave spectra were expressed in terms of energy and called wave-energy spectra which commonly $a^2/2$ or simply a^2 is plotted along the vertical axes. The wave energy spectrum is synonym to the variance spectrum.

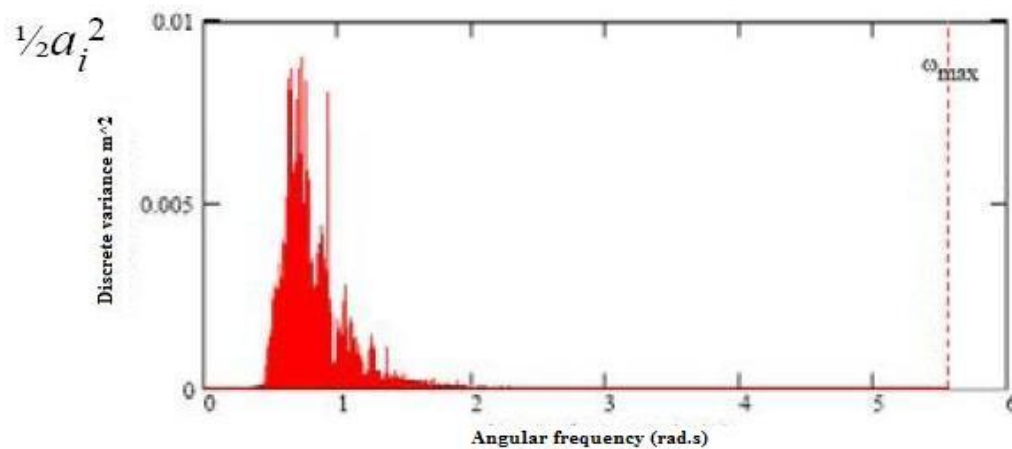


Figure 5: Discrete variance spectrum or wave energy spectrum

A wave spectrum is the distribution of wave energy over frequency. The form of the spectrum is usually expressed in terms of the moments of the distribution (spectrum). The n th-order moment, m_n , of the spectrum, approximated by a finite sum, is:

$$m_n = \sum_{i=0}^N f_i^n \frac{a_i^2}{2}$$

According to the definition of m_n , the zero moment, m_0 , represents the area under the spectral curve, which in case of energy spectrum is the total energy in the wave field (E). The so called root-mean-square wave height (H_{rms}) is defined in respect to this.

$$m_0 = \sum_{i=0}^N \frac{a_i^2}{2} = \frac{a^2}{2}$$

$$E = \frac{1}{8} \rho_w g H^2 = \rho_w g \frac{a^2}{2}$$

$$H_{rms} = \sqrt{\frac{8E}{\rho_w g}} = \sqrt{8m_0}$$

In order to derive a value for wave height from the spectrum, as close as possible to the significant wave height $\bar{H}_{1/3}$ (as derived directly from the wave record), it has been shown that the H_{rms} must be multiplied by the factor of $\sqrt{2}$ for arriving at the required value.

$$H_s = \bar{H}_{1/3} = \sqrt{2} \sqrt{\frac{8E}{\rho_w g}} = 4\sqrt{m_0}$$

The commonly used parameters from the spectral wave frequency and wave period, derived from the wave spectrum are:

f_p = wave frequency corresponding to the peak of the spectrum

T_p = Wave period corresponding to f_p

T_{m01} = Wave period corresponding to the mean frequency of the spectrum:

$$T_{m01} = \frac{m_0}{m_1}$$

T_{m02} = Wave period theoretically equal to mean zero-crossing period \bar{T}_z :

$$T_{m02} = \sqrt{\frac{m_0}{m_2}}$$

The wave spectrum defines the sea state. In order to express the wave spectrum as a functional form, some models of the spectrum are used, usually in terms of frequency, $E(f)$, frequency and direction, $E(f, \theta)$, or alternatively in terms of wave number, $E(k)$. They are used to obtain an estimate of the whole spectrum from the limited number of known parameters such as significant wave height and wave period. There exist many different models such as the *Phillips' spectrum*, the *Pierson-Moskowitz spectrum, PM*, (which is often used for a fully developed sea especially when duration and fetch are unlimited), and the *JONSWAP spectrum*. The last mentioned spectrum is often used for describing the waves in a growing phase (WMO, 1998).

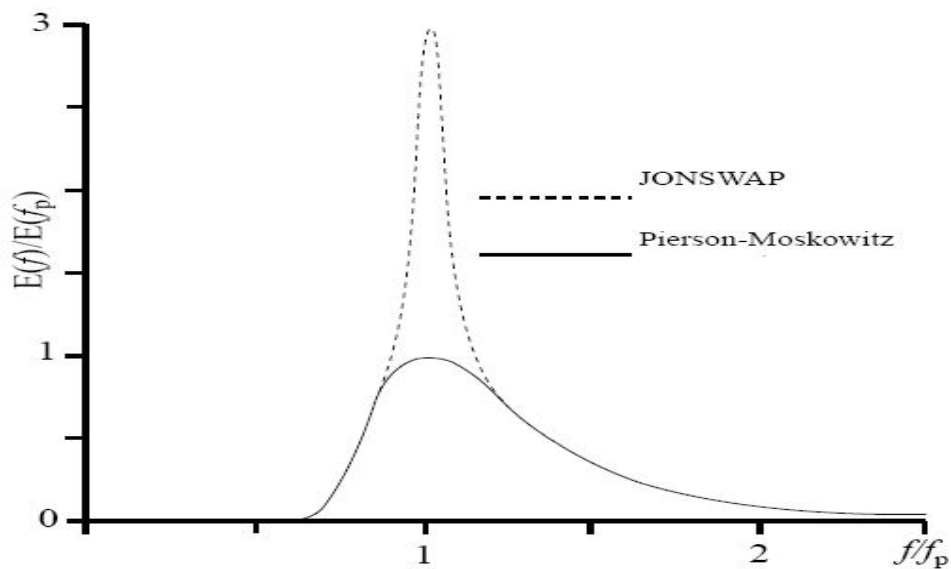


Figure 6: JONSWAP and PM spectrum models

2.2 Wave modelling

Importance of wave characteristics in different fields such as the naval industry and coastal and offshore constructions has led to development of various modelling techniques. Significant efforts to model and predict the waves were made in the Second World War and remarkable developments have since been achieved.

The first wave models were empirical prediction methods. The main concept of these methods is the relationship between dimensionless wave parameters governed by universal laws of fetch and duration limited growth. SMB, PNJ and PM were the first series of empirical methods predicting both spectra and their integral properties such as significant wave height, peak frequency, etc. (Silvester, 1974).

Although the above approaches are useful, they are limited to a narrow range of applications (fetch and duration limited growth). To involve all physical processes that occur in nature, such as local wind generated sea and swell, spatially and temporally varying winds and irregular bathymetry and coastlines, more comprehensive models must be used. These will by necessity be numerical models. (Young, 1999)

Numerical models for describing wind wave evolution can be divided into two general classes: first are the phase resolving models, which represent the time varying water surface, resolving both the amplitudes and phases of the individual waves. Second are phase averaging or spectral models which predict average quantities such as the directional wave spectrum or its integral properties. The directional wave spectrum defines the distribution of wave energy with frequency and direction. Phase averaging models solve a single equation:

$$\frac{\partial F}{\partial t} + C_g \cdot \nabla F = S_{tot}$$

Where $F=F(f,\theta,x,y,t)$ is the directional spectrum of the waves and C_g is the group velocity vector. The symbols f , θ , x , y and t denote frequency, direction, horizontal Cartesian coordinates and time, respectively. The source term S_{tot} is the summation of different processes which in the simple case of deep water will be:

$$S_{tot} = S_{in} + S_{nl} + S_{ds}$$

Where S_{in} is the external gain as atmospheric input from the wind, S_{nl} is the shifting of energy within the spectrum due to nonlinear wave-wave interactions and S_{ds} is dissipative loss.

Representation of the source term S_{tot} is related to the level of understanding the physical process causing the wind-wave evolution. This has classified the models into three categories of first, second and third generation models.

First generation models were established before development of nonlinear wave-wave interactions and the source term contained only atmospheric input and dissipation. The atmospheric input in these models is based on Phillips' resonance mechanism and Miles' shear flow mechanism (mentioned mechanisms will be discussed later in this section). There are some disadvantages using first generation models. For instance,

they give good results only for regions for which they have been developed and calibrated.

Second generation models were developed after the important role of nonlinear wave-wave interactions became clear in the JONSWAP studies. As a result, a parametric representation of nonlinear interactions, S_{nl} , was included in the source terms. Inclusion of nonlinear wave-wave interactions effects enhanced the modelling capability. Also in demanding situations such as hurricanes, reasonable results were produced. In the atmospheric input, only Miles' mechanism is taken into account as Phillips' resonance mechanism has a very small effect. However, the role of Phillips' model cannot be ignored in the initial growth of the waves from a calm sea. This was considered by defining the initial conditions for the model.

In 1984 the WAM (WAVE Modeling) Group initiated by Klaus Hasselmann, developed a third generation model. The source term balance in third generation models is the same as second generation models. The details of the source terms are, however, significantly different to second generation models. The outcome from WAM Group was the WAM Model. A variant of this basic model was developed by Tolman (WAVEWATCH) and more recently Booij developed the SWAN model. (Young, 1999)

More details about the source terms in first, second and third generation models can be found at Young, I.R. (1999), *Wind Generated Ocean Waves*.

2.3 Wave generation

Wind-waves are generated by the winds blowing over the water surface. The wave growth is mainly dependent on the wind speed, the distance (fetch) over which a propagating wave is influenced by the wind and the duration of the wind. When the wind ceases or waves leave the windy generation area, the waves are called swell. Swells have different characteristics than wind waves. They are smoother due to dissipation and have longer crests. (Wiegel 1964, WMO 1998)

There are two stages in wind-wave generation which are recognized by distinct mechanisms; these are: (1) resonance, produced by air pressure fluctuations on the water surface; (2) shear flow, by the wind-velocity profile above the water surface.

The wind input term; S_{in} is generally defined as the form:

$$S_{in} = A(f, \theta) + B(f, \theta)E(f, \theta)$$

$A(f, \theta)$ is the resonant interaction between waves and turbulent pressure patterns in the air, whereas the second term represents the shear flow growth mechanism. (Silvester, 1974)

2.3.1 Resonance

This mechanism and the related theory of wave initiation by resonance of the water surface were developed in 1957 by O.M. Phillips (Phillips, 1957, cited by Silvester, 1974). Movement of air in the form of wind is always associated with random fluctuations of pressure and velocity about some mean value, or turbulence. They are the results of swirls or turbulent eddies in the moving mass of the air. These eddies create random fluctuations of pressure and of shear on the water surface. Phillips' theory only considers the pressure fluctuations in the vertical direction.

The depression caused by the pressure from the eddy is quite short and instant, but it creates a wave with a specific wave height. However if the pressure remains on the created trough, it will grow deeper and so the wave will grow. The concept of resonance is defined by the matching of the speed of the wave first initiated to that of the eddy producing it. For the specific depth of water any created wave length has a given wave speed.

$$c = \sqrt{\frac{g}{k} \tanh kh}$$

$$k = \frac{2\pi}{\lambda}$$

c : Wave speed

g : Acceleration of gravity

h : Depth

k : Wave number

λ : Wave length

The resonance theory of Phillips' does not consider the effect of waves on the air flow after they are generated. Therefore it can only explain the initiation of waves. This source term is of the form:

$$A(f, \theta) = \frac{2\pi^2 \omega}{\rho_w^2 c^3 c_g} \Pi(k, \theta)$$

where $\Pi(k, \theta)$ is the three dimensional wave number, frequency spectrum of atmospheric pressure. (Silvester, 1974)

2.3.2 Shear flow

This theory was devised by J.W. Miles in 1957 (Miles, 1957, cited by Silvester, 1974) almost simultaneously with that of Phillips. It is not substituting the resonance model, but complements it.

The model assumes an initial disturbed surface with sinusoidal waves of infinite crest. This will cause a kind of waviness in the streamlines of air flow near the surface. This

compression and spreading of the streamlines has the same speed as the wave celerity C . Assuming a distribution for the wind velocity $U(y)$ as in Figure 7, subtraction of it from the wave celerity C results in a zero point at the height y_c . In the critical zone below y_c the air velocity is reversed in respect to the wave celerity. In this critical zone a strong vortex is established which drains energy from the wind at the same rate as it is transferred to the wave.

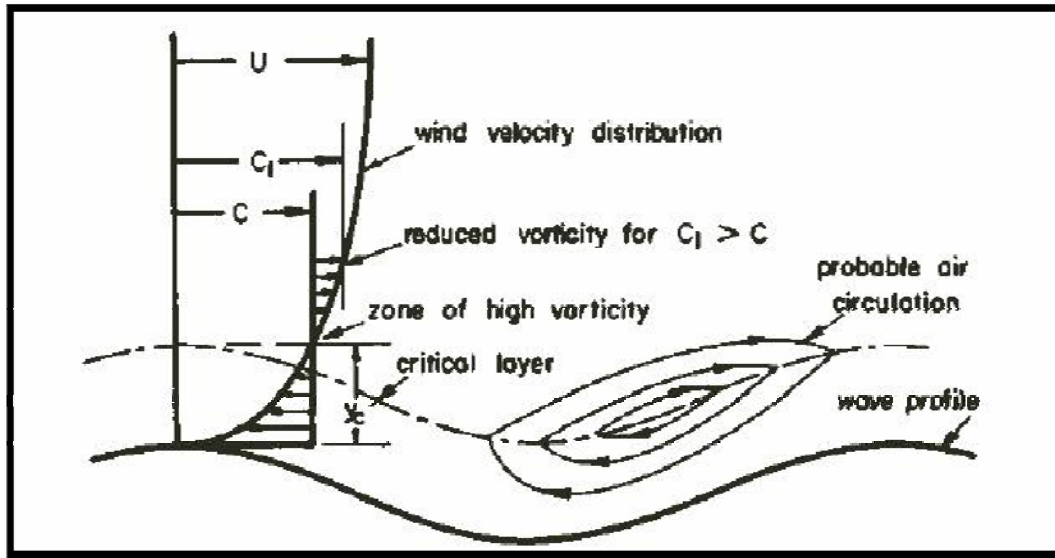


Figure 7: Definition sketch for shear flow model of wave generation

The rate of this growth is exponential and is described in terms of the wave energy spectrum:

$$E(f, \theta) = \frac{k}{4\pi f \rho_w^2 \mu g} P(k, f) (e^{2\pi f t \mu} - 1)$$

or

$$\frac{\delta E(f, \theta)}{\delta t} = B(f, \theta) E(f, \theta) = 2\pi f \mu E(f, \theta)$$

where $E(f, \theta)$ is a frequency-direction component, k is the wave number, $P(k, f)$ is the spectrum of wave-induced turbulence, μ is a coupling coefficient to be defined, g is gravitational acceleration and ρ_w is the water density.

The growth rates predicted by Miles were much smaller than those from observations and laboratory and field tests. Based on a field experiment, Snyder and Cox (1966), cited by WMO (1998), proposed a coupling coefficient, μ , as follows:

$$\mu = \frac{\rho_a}{\rho_w} \left[\frac{u}{c} \cos(\theta - \psi) - 1 \right]$$

where c and θ are the wave speed and direction of the growing component, ψ and u are the direction and speed of the wind and ρ_a is the air density.

A revision was proposed by Snyder et al. (1981), cited by WMO (1998), which is:

$$B(f, \theta) = \max \left[0, K_1 2\pi f \frac{\rho_a}{\rho_w} \left(\frac{U_5}{c} \cos(\theta - \psi) - 1 \right) \right]$$

The wind speed at the original work was measured at the height of 5 meters. In order to generalize this equation, the wind input shall be expressed in terms of friction velocity:

$$u_* = \sqrt{\frac{\tau}{\rho_a}} = u \sqrt{C_d}$$

where τ is the wind stress and C_d is the drag coefficient. The drag coefficient varies with u . Komen et al. (1984), cited by WMO (1998), has used an approximate form describing the input source term:

$$B(f, \theta) = \max \left[0, K_1 2\pi f \frac{\rho_a}{\rho_w} \left(K_2 \frac{u_*}{c} \cos(\theta - \psi) - 1 \right) \right]$$

where $K_1 \approx 0.25$ and $K_2 \approx 28$ are the constants which give some flexibility to this term. (Silvester, 1974 - WMO, 1998)

2.4 Wave dissipation

The dissipation of wave energy can be caused by three different processes: surf breaking, wave-bottom interaction and white-capping. Surf breaking only occurs in very shallow water where depth and wave height are of the same order. Dissipation of wave energy due to wave-bottom interaction is due to bottom friction. White-capping is the primary mechanism of the wave energy dissipation in deep and open oceans. The dissipation term is generally defined as the form:

$$S_{ds} = S_{br} + S_{bf} + S_{wc}$$

where S_{br} is the dissipation source term for surf breaking, S_{bf} represents bottom friction dissipation and S_{wc} is the white-capping dissipation source term.

2.4.1 Wave breaking in the surf zone

In very shallow water where the depth is in the order of the wave height, the upper part of the wave increases its speed relative to the lower part. At some point the crest speed gets sufficiently high to overtake the preceding trough. The wave face becomes unstable and water from the crest falls along the forward face of the wave. There are four types of breaking water waves: spilling, plunging, collapsing and surging breakers.

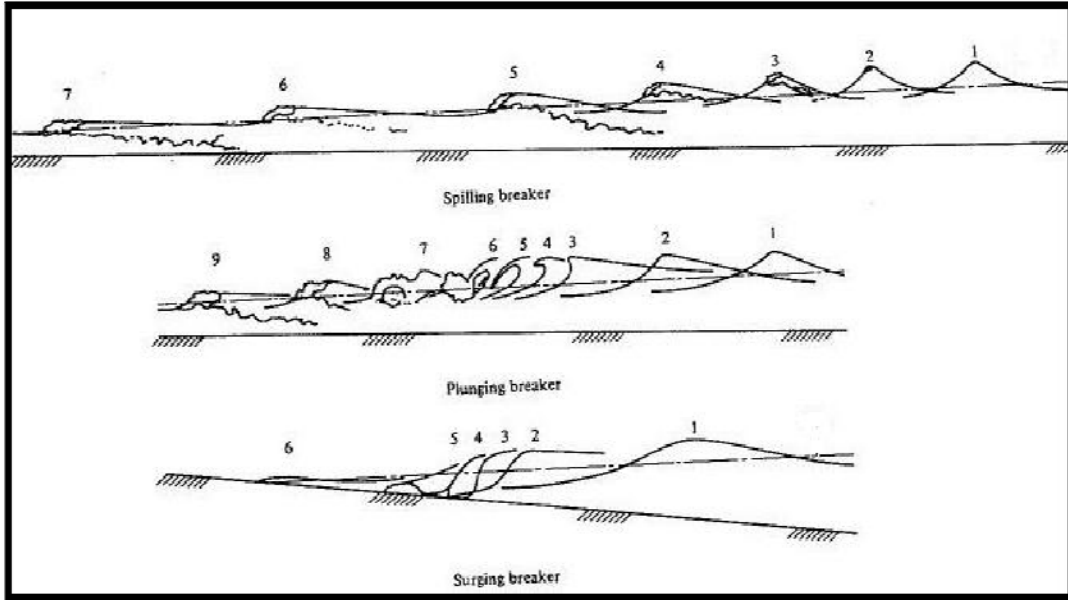


Figure 8: Three types of wave breaking on beaches, Small figures denote different stages of the breaking process

Batjes and Janssen (1978) considered all waves above limiting height, H_{max} were breaking. Also the waves below this height followed a Rayleigh probability density distribution as:

$$P(H) = \frac{H}{4\sigma^2} e^{-\frac{H^2}{8\sigma^2}}$$

where σ^2 is the variance of the wave record. Therefore the probability that the wave height is greater than H_{max} is:

$$Q_b = P(H > H_{max}) = e^{-\frac{H_{max}^2}{8\sigma^2}}$$

where Q_b is the fraction of waves which are breaking. According to the definition of H_{rms} , Q_b can be calculated as below:

$$H_{rms}^2 = \int_0^{\infty} H^2 p(H) dH = 8\sigma^2$$

$$H_{rms}^2 = \int_0^{H_{max}} H^2 p(H) dH + Q_b H_{max}^2 = 8\sigma^2(1 - Q_b)$$

Eliminating σ^2 between x and x yields:

$$\frac{1 - Q_b}{\ln(Q_b)} = - \left[\frac{H_{rms}}{H_{max}} \right]^2 = -8 \frac{E_{tot}}{H_{max}^2}$$

Source term for breaking in the spectral energy balance, based on Battjes and Janssen (1987) is then:

$$S_{br}(f, \theta) = -\frac{1}{4} \alpha_{bj} f_p Q_b H_{max}^2 \frac{E(f, \theta)}{E_{tot}}$$

where α_{bj} is an empirical coefficient of the order one, f_p is the peak frequency and E_{tot} is the total wave energy. (Young, 1999)

2.4.2 Bottom friction

Dissipation at the sea-bed can be modelled by the action of stress, τ , on water with the velocity of u_b just above the bottom boundary layer.

$$\tau = -C_f \rho_w u_b |u_b|$$

where the bottom friction coefficient, C_f , may be expected to vary slowly with flow conditions. Hasselmann and Collins (1968) have analyzed the relationship between the bottom stress and the dissipation rate of each spectral component. A simplified equation for the dissipation source term is:

$$S_{bf}(f, \theta) = -C_f \frac{\omega^2 E(f, \theta)}{g^2 \sinh^2 kh}$$

where ω is the angular frequency, k is the wave number and h is the water depth. The bottom coefficient, C_f , is equal to 0.038 for swell conditions and 0.067 for the wind-wave conditions. (Young, 1999)

2.4.3 White-capping

The increase in the wave amplitude due to input of energy by wind continues until the wave eventually becomes unstable and breaks. This is called white-capping in contrast to surf breaking which occurs on a beach.

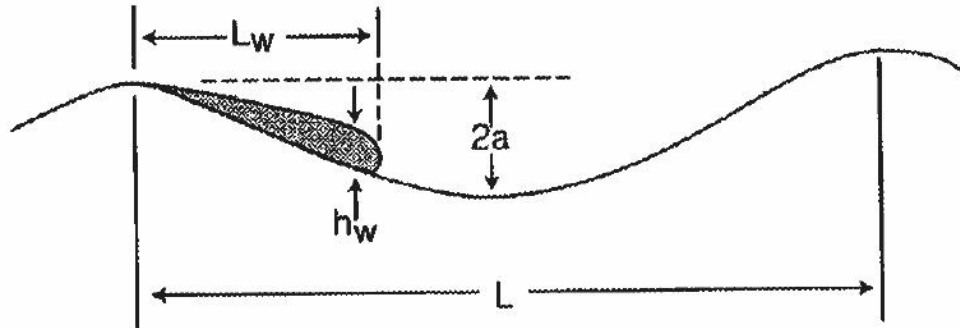


Figure 9: The geometric similarity of the white-cap and the underlying wave, where h_w is the height and L_w is the length of the white-cap region

As the wave starts breaking, the energy dissipates in two ways: water is injected into the white-cap, becoming turbulent and interacting with the orbital flow on the forward face of the wave. The presence of the white-cap on the forward face of the wave extracts energy from the wave. This dissipation depends on the existing energy of the waves and the wave steepness, and can be written:

$$S_{wc}(f, \theta) = -\gamma_{ds}\omega E(f, \theta)$$

where γ_{ds} is a damping coefficient which is a function of non-local properties of the spectrum. (Young, 1999)

2.5 Nonlinear wave-wave interactions

To first order, waves can be considered as the superposition of independent spectral components. However at higher orders, interactions, or in another word, kind of resonance happens between components and they are not independent. This results in a transfer of energy between the components. The lowest order that such interactions may occur is between three waves, triad interactions. The most general case which is more significant in deep waters, involves the interaction between four components, called quadruplet interactions.

Triad (three-wave) interactions are significant in shallow water. They can occur between the wave components which their frequency and wave number satisfy the following conditions:

$$f_1 \pm f_2 = f_3$$

$$k_1 \pm k_2 = k_3$$

where f_i is the scalar frequency and k_i is the vector wave number, of the i th wave component. These resonant wave-wave interactions transfer and redistribute the energy between these components in such a way that preserves some characteristics of the spectral shape and the total energy in the wave field. The resonance which causes this transfer between components can be expressed by putting the conditions that the frequencies of the interacting waves must sum to zero, and the same for the wave numbers.

More significant in deep waters is the interaction of four waves, called a quadruplet, which could exchange energy when the following conditions are satisfied:

$$k_1 + k_2 = k_3 + k_4$$

$$f_1 + f_2 = f_3 + f_4$$

The complicated cubic integrals which describe these energy transfers are:

$$S_{nl}(f, \theta) = f \iiint dk_1 dk_2 dk_3 \delta(k_1 + k_2 - k_3 - k_4) \delta(f_1 + f_2 - f_3 - f_4) [n_1 n_2 (n_3 + n_4) - n_3 n_4 (n_1 + n_2)] K(k_1, k_2, k_3, k_4)$$

where the delta functions, δ , enforce the resonance conditions, the (f_i, k_i) for $i=1, 2, 3$ are the frequency and the wave number pairs for the interacting wave components, the $n_i = \frac{E(f_i, \theta_i)}{f_i}$, are the wave action densities, and the Kernel function, K , gives the magnitude of the energy transfer to the component k_4 , (or (f_4, θ)) from each combination of interacting wave components. (Young, 1999 – WMO, 1998)

2.6 Coriolis Effect

All spots on the Earth have the same angular velocity, but different linear velocity regarding their location on the Earth. The minimum linear velocity is at the poles. Getting closer to the equator, the radius of rotation gets bigger and therefore the linear velocity increases. So by moving from poles toward equator or vice versa the linear velocity changes, which means there is acceleration and therefore there is force acting. This force is called the coriolis force. This deflecting force can affect the progressive and standing waves. The effect of this phenomenon is more significant on

waves with periods of the order of magnitude of the period of inertia oscillations, such as half a pendulum day. Seiches and tidal waves fit more into this range of period than the wind waves. Time, space and velocity are three important factors influencing the effectiveness of Coriolis force. This can be determined by calculating the Rossby number:

$$R = \frac{U}{fL}$$

$$f = 2\Omega \sin \phi$$

where U is the velocity of the system, L is the length scale of the motion f is the Coriolis parameter, Ω is the angular velocity of planetary rotation and ϕ is the latitude. The Rossby number can range between 0.1-1 and 1000. Big values of Rossby number means the Coriolis force have small or negligible effects. (Kantha & Clayson, 2000 - Dietrich, 1957)

In this project, regarding the wave characteristics in the region that focuses on wind waves, considering the Coriolis Effect would be unnecessary.

2.7 SWAN

SWAN (Simulating WAVes Nearshore) is a phase averaging third generation model, solving the single equation of wave action balance. Based on the deep water third generation WAM Model, it has additional capability of taking the shallow water effects into account such as Triad wave-wave interactions, depth induced breaking and bottom friction. SWAN is meant to be used in coastal and shallow areas, lakes and estuaries by modelling the wave propagation from deep water into shallow coastal regions (The SWAN team, 2008). Although in big scale simulations and open oceans, the WAM and WAVEWATCH models are more computationally efficient than the SWAN model, but the great flexibility in modelling and tuning physical processes, either in shallow or deep water makes SWAN the most appropriate wave model currently. (Rusu, 2009)

Wave parameters are estimated in SWAN from given wind, bottom, water level and current conditions. In general two types of computational grids are considered in SWAN: structured and unstructured. Structured grids contain quadrilaterals with 4 cells meeting at each internal grid point. Unstructured grids can contain triangular cells or a combination of triangular and quadrilateral cells. At the moment only triangular meshes can be employed in SWAN via a few supported meshing codes, one such is TRIANGLE. (The SWAN team, 2008)

Significant wave height (H_S) and mean zero crossing wave period (T_{m02}) are the two main output parameters from SWAN in this project.

3 Method

3.1 Nesting

The idea of nesting is to first compute the waves on a coarse grid for a larger region and then on a finer grid for smaller regions. The computation on the smaller grid uses the boundary conditions generated by the computation on the coarse grid. In this project, the large region is the Baltic Sea, Skagerack and Kattegatt. The coarse grid resolution is 6×6 NM. The small region is located at the east coast of Sweden in the Baltic Sea, covering the Ölands and Gotland Islands, starting above Stockholm, going down close to the Polish coast. Trial and errors in order to find the optimum computational grid resolution take place in the small nested region.

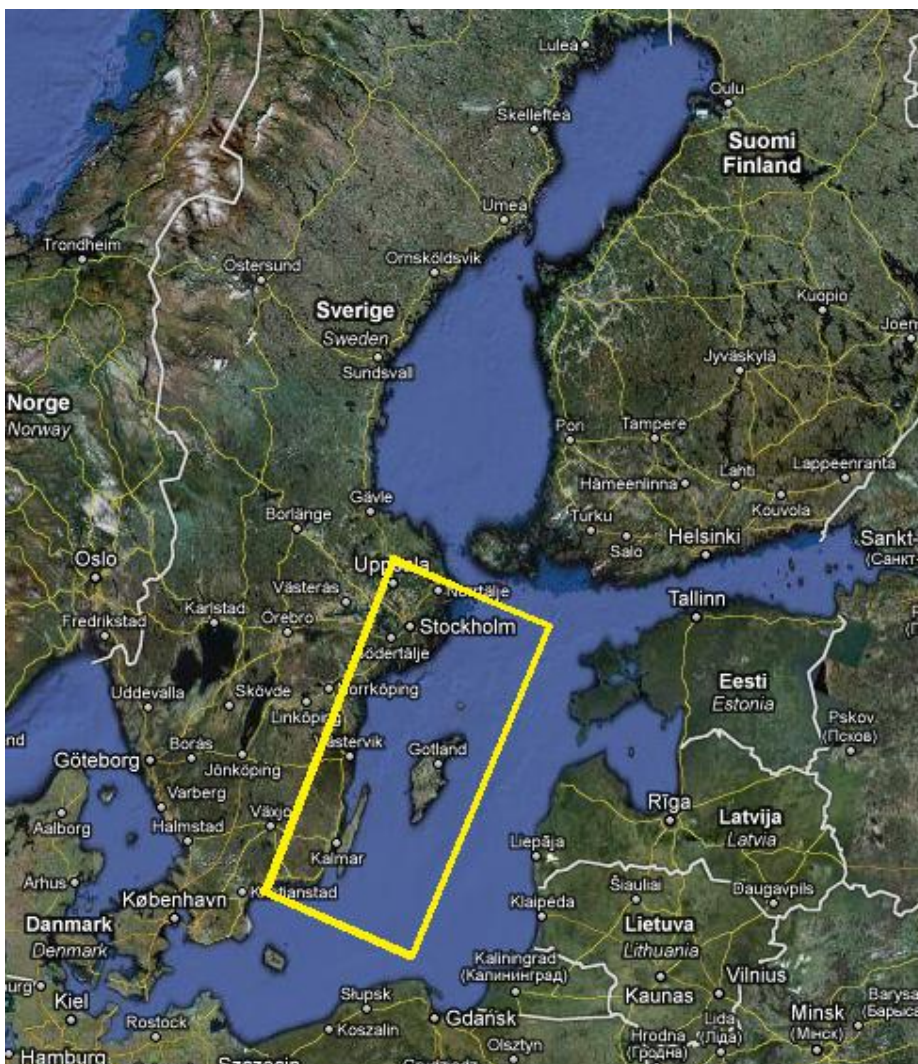


Figure 10: The whole region and the nested area

3.2 Coordinate system and grid translation

A relatively large area of the Earth surface is covered in this project, which makes the Earth curvature become noticeable and the use of a spherical coordinate system inevitable. The WGS 84 (decimal degrees) coordinate system is used in this work. All input data are in the same system as well.

By getting closer to the poles in a spherical coordinate system, the curvature of longitudes become more significant and grid cells with same west-east decimal degree distances do not have the same size. In order to have almost rectangular grid cells, one must translate the grid to the equator. This will keep the distance between grid cells approximately the same.

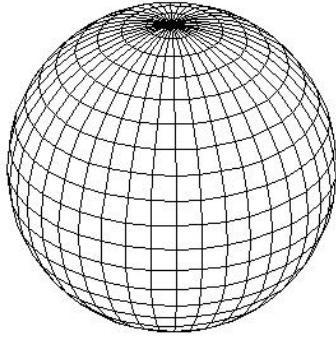


Figure 11: Latitudes and longitudes at spherical coordinate system

In order to have a rectangular region after translation, a backward translation is used, and the quadrilateral area after translating to the equator has become a perfect horizontal rectangular area, see Figures 12 and 13.

The coordinates of the South Pole have been rotated to (-10, -30), and all other points have been rotated respectively:

$$y_{rot} = \sin^{-1}[\cos(y_c + 90) \sin(y_{reg}) - \sin(y_c + 90) \cos(y_{reg}) \cos(x_{reg} - x_c)]$$

$$x_{rot} = \cos^{-1} \left\{ \frac{[\sin(y_c + 90) \sin(y_{reg}) + \cos(y_c + 90) \cos(y_{reg}) \cos(x_{reg} - x_c)]}{\cos(y_{rot})} \right\}$$

where (x_c, y_c) are the translated coordinates of the South Pole, (x_{reg}, y_{reg}) are original coordinates of the grid points and (x_{rot}, y_{rot}) are translated coordinates of the grid points. All coordinates are in geographical (longitudes and latitudes) system.

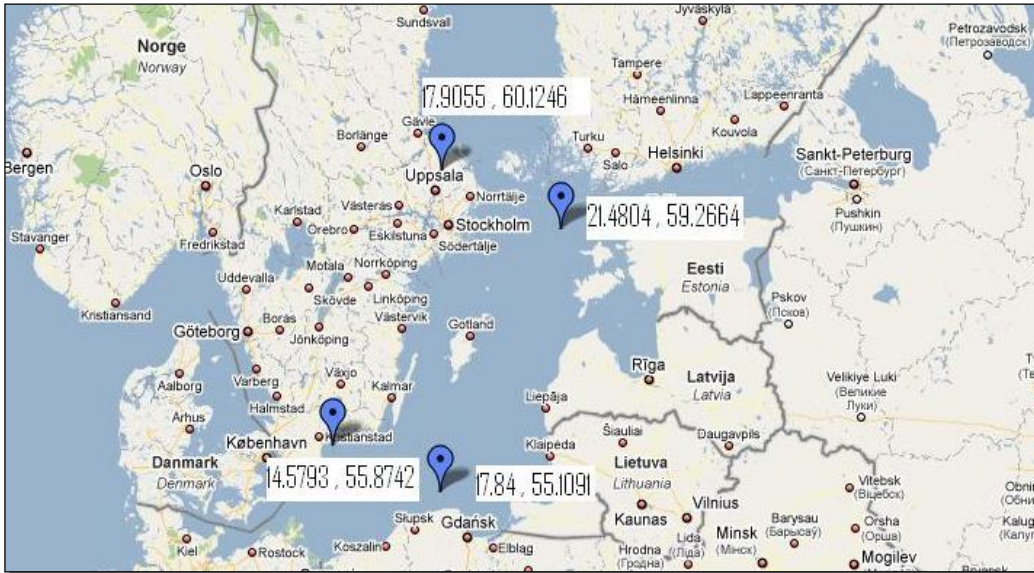


Figure 12: Nesting region before translation

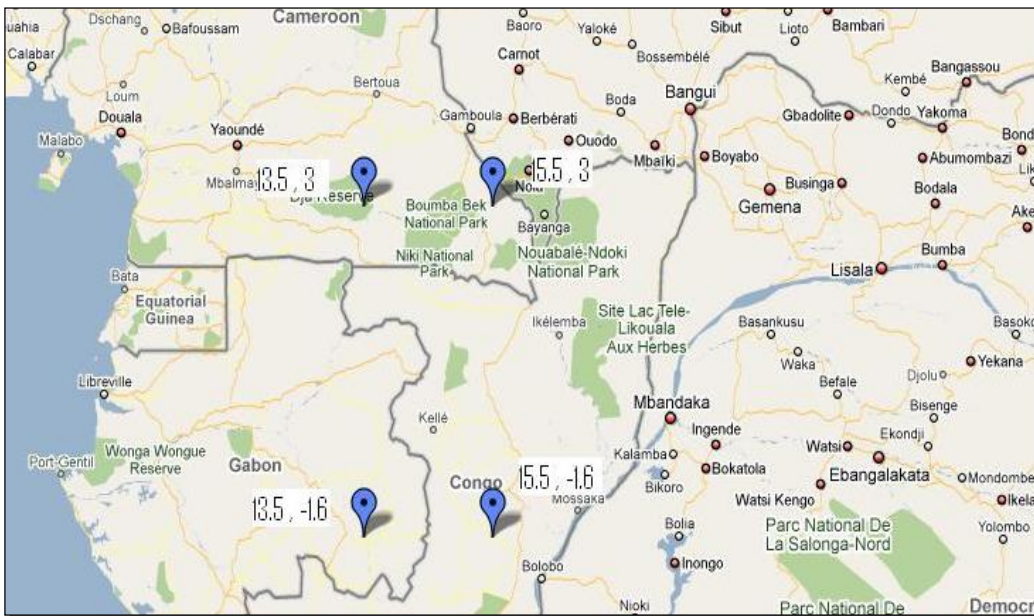


Figure 13: Nesting region after translation to the equator

3.3 Computational Grids

Two different types of computational grids have been used for the small nested region. One is an unstructured, and the other is structured with different resolutions.

3.3.1 Unstructured grids

The advantage of using unstructured grids is to have varying resolution in the same grid. This makes the computations more efficient. There will be higher resolution in coastal areas and less in the open sea. To use unstructured grids in SWAN, the mesh must be provided in advance. There are few meshing codes which are supported by SWAN. In this work, the TRIANGLE mesh generator was used.

TRIANGLE is a two dimensional high quality triangular mesh generator code, developed by Jonathan Richard Shewchuk at Computer Science Division, University of California at Berkeley. It creates Delaunay triangles using points given by the user as their vertices. If the minimum requirements for a perfect triangle (angles and area) are not satisfied, TRIANGLE can produce more vertices to reach any required limit (Shewchuk, 1996).

Figure 4 shows the triangulated nested region, which will be imported to SWAN as unstructured computational grid. It has 9126 triangles which include 5427 vertices, of which 1985 are input and the rest are produced by TRIANGLE in order to fulfil the high quality Delaunay triangulation limits.

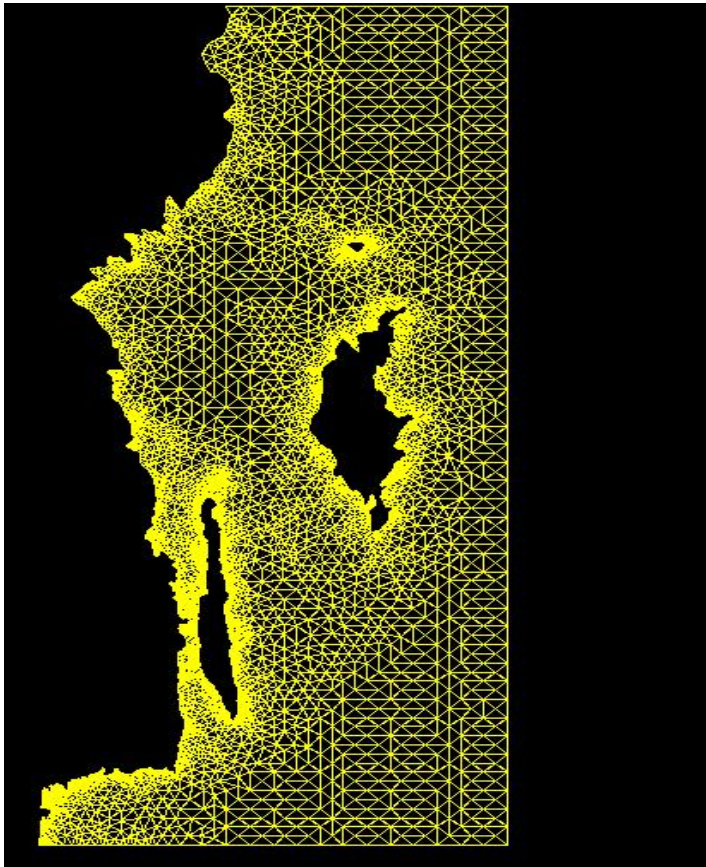


Figure 14: Unstructured meshing of the small nested region by TRIANGLE

3.3.2 Structured grids

The previous simulation in 2008 had a structured computational grid of 6×6 NM. One possible way to improve the results is to use finer computational grids. In this case three different resolutions of 1.2×1.2 NM, 2.0×2.0 NM and 3.0×3.0 NM were applied to find an optimum resolution. The nested area has dimensions of 2.0×4.6 degrees, which is 120×276 NM. This means we will have grids with 23000, 8280 and 3680 vertices respectively. Figure 15 shows the 3 NM grid covering the nested region.



Figure 15: 3NM structured grid covering the whole region

3.4 Physics

There are different physical phenomena which influence the wave propagation. The simulation in SWAN is done under third generation mode for wind input, considering quadruplet and triad wave-wave interactions and white-capping dissipation. Westhuysen white-capping source term, which is a nonlinear saturation-based white-capping combined with wind input of Yan is chosen, as it has been proven to give much better results. (Hoque et al., 2009)

In shallow areas which waves start to be influenced by the sea bed, bottom friction has a significant impact on their propagation. The friction formulation of Hasselmann has been used in SWAN model with constant friction coefficient of $0.067 \text{ m}^2/\text{s}^3$ which is for the wind-wave conditions. (The SWAN team, 2008)

3.5 Input data

3.5.1 Wind

For the atmospheric forcing, the RCA 3.0 wind data base has been used. RCA is the Rossby Centre regional Atmospheric climate model covering great parts of Europe with a resolution of either 25 km or 50 km. It uses boundary conditions from the ECMWF (European Centre for Medium-Range Weather Forecasts) reanalysis experiment ERA40.

The data base covers more than 40 years (1961 to 2005) including wind velocity and 3-second gusts every three hours. RCA is capable for both providing hindcast and future winds based on global climate change scenarios on the boundaries. Because of underestimation of wind speed during extreme events, 3-second gust was used to adjust the output wind velocity in RCA 3.0. In this project a fifteen year period of RCA3.0 (1990-2004) hindcast winds is used. The database has a grid resolution of about $12 \times 12 \text{ NM}$. The same set of data was used in the previous simulation in 2008. Therefore the wind input file from year 2008, which also has been translated to the equator, is used directly in this project. (Broman & Kriezi, 2008)

3.5.2 Bathymetry

HIROMB (High Resolution Operational Model for the Baltic Sea) bathymetric data base, with resolution of $1.0 \times 1.6 \text{ NM}$ is used in this project. It is a combination of different bathymetric databases from the countries around the Baltic. For the nested runs in the small region, bathymetric data from Sea Charts have been combined with this database to have more local precision.

3.5.3 Ice coverage

In the northern parts of the Baltic Sea there are periods during the year when ice covers the sea. There is no source term included in SWAN to calculate dissipation due to ice neither any other technique to treat ice. Same as what has been done for 2008, whenever the ice concentration is above 50% it is considered as land; otherwise the ice is considered as water. This has been done by using the “Water Level” switch in SWAN. (Broman & Kriezi, 2008)

3.5.4 Boundary conditions

Except for the western boundary of the project area, which is connected to the North Sea, the rest of the boundary consists of land. A coarse structured grid (12×12 NM) simulation covering the North Sea and parts of Skagerack is first introduced. Subsequently the main simulation uses spectral boundary conditions from the coarse one.

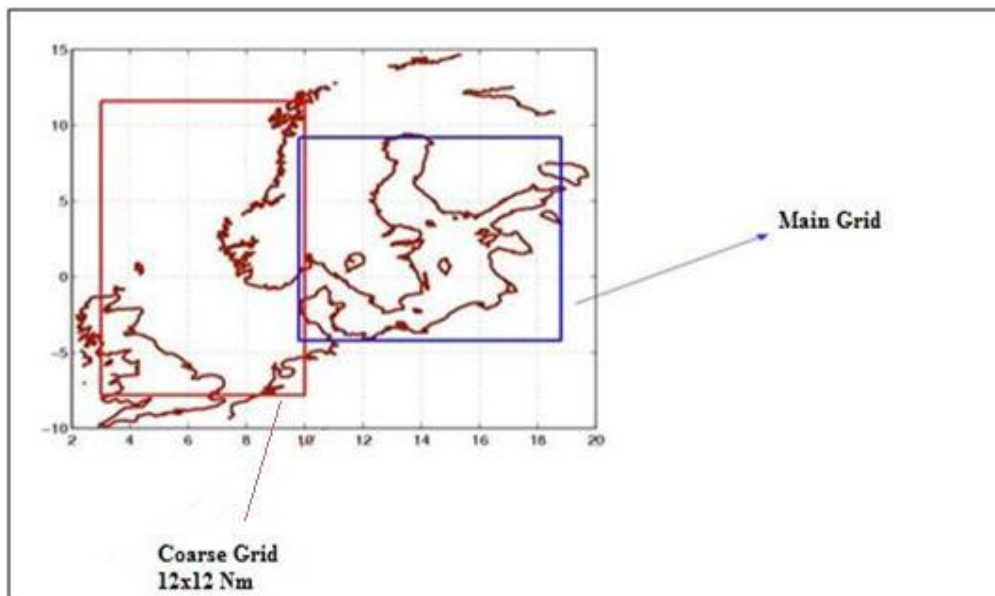


Figure 16: Grids location

3.6 Measured data sources

The simulation results will be evaluated by comparing them with the recorded data at measurement stations. Two different types of measurement devices, buoys and bottom-fixed devices have been used at measurement stations in coastal areas around Sweden since three decades ago. An inverted echo-sounder from SimRad and an analogous device (WHM) are two types of the bottom-fixed devices (Broman et al., 2006). One type of the Buoys (the floating measurement devices) is Waverider (Datawell[®] oceanographic instruments).

The measurement stations which were operating discontinuously during the period of 1990-2004 are Almagrundet, Ölands Södra Grund, Kristianopel, Fladen and Trubaduren. They record the wave characteristics every one hour. The recorded data include significant wave height, mean wave period, first, second, third, fourth and fifth largest wave heights and wave spectrum.



Figure 17: Different measurement devices, from left, Simrad, Waverider and WHM

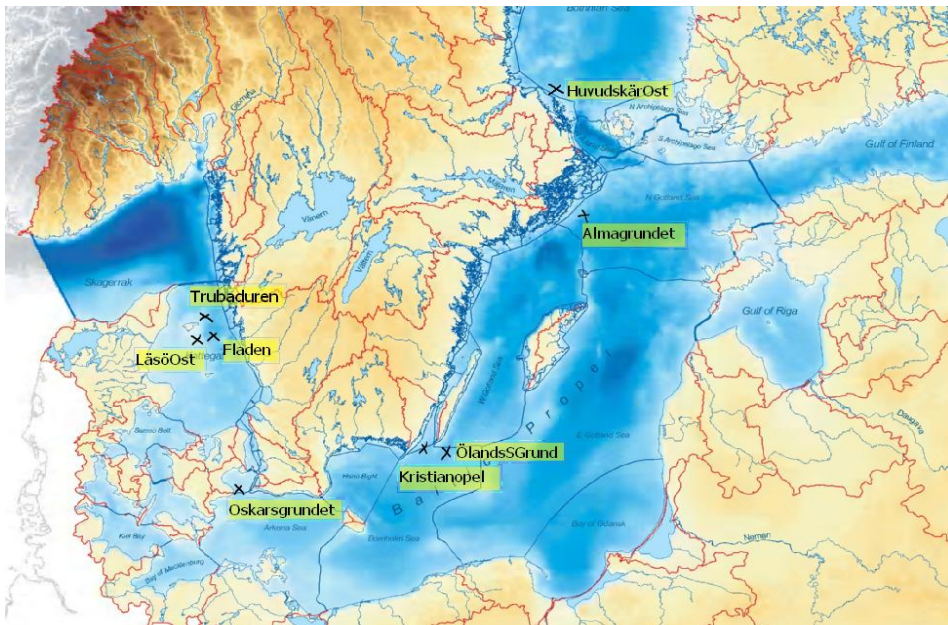


Figure 18: Location of the measurement stations

3.7 Parallel processing

To run a problem using one processor, the problem is divided into small portions and each portion will be processed one after another by the CPU. But when there is a bigger problem, such procedure would be inefficient. One solution is to decompose the problem and run each part in a separate processor at the same time while they are communicating with each other as well. This is called parallel processing. Figures 19 and 20 show a very basic schematic of how parallel processing looks as compared to a serial processing.

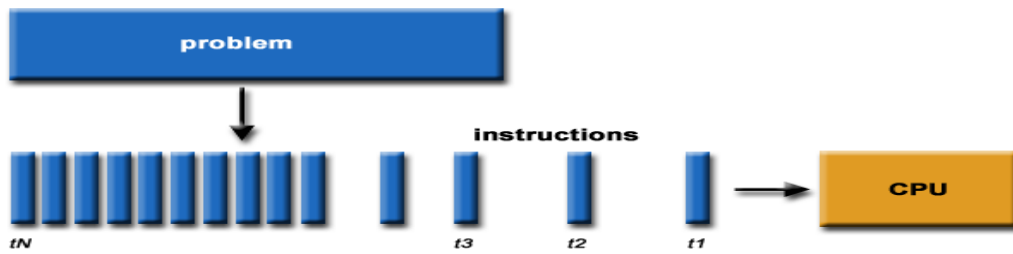


Figure 19: Basic schematic view of serial processing

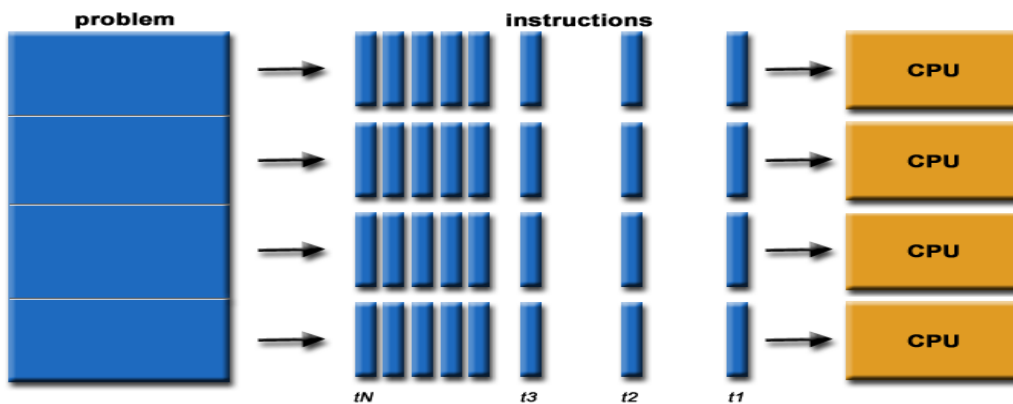


Figure 20: Basic schematic view of parallel processing

In order to run the simulations faster, SWAN is used in parallel mode. In this parallelization method, the domain is decomposed and each sub-domain can have multiple neighbours on each side. There will be a data structure to store all the information about the relationship of the sub domain and its particular neighbours. In parallel processing all processors must communicate and exchange information. In SWAN both MPI and OpenMP can be used for this communication. Using MPI, it is possible for different nodes to communicate, while OpenMP only makes it possible for all kernels at one node to communicate. When using OpenMP, the kernels cannot communicate with kernels at other nodes (The SWAN team, 2008).

At the available cluster at SMHI, each node has 8 kernels and each kernel can run 1 process. The 8 kernels share the memory space at their own node. If we like to run a case using more than 8 kernels we need to link to the MPI-libraries when compiling.

For running the coarse grid over the North Sea and the small nested region OpenMP has been used. For the whole main region with the optimum resolution MPI libraries are used.

4 Results

4.1 Calibration

The results from October 1990 at Almagrundet measurement station are presented here. The general features are similar for the rest of the year. In Figures 7 and 8, significant wave height and mean wave period from different scenarios are plotted together with measurements. The results from the three simulations with structured computational grids have better matching with measurements than results from the simulation with unstructured computational grid. Only in periods with strong wind it shows reasonable wave heights.

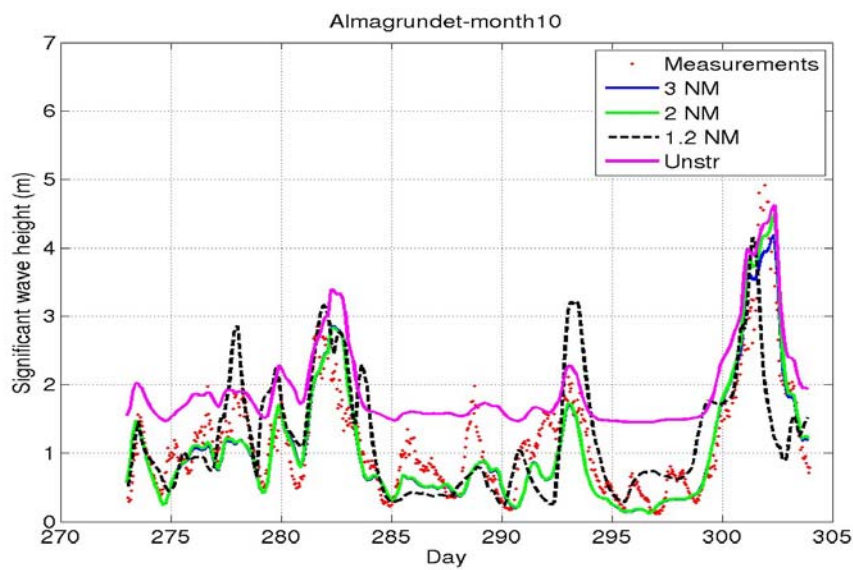


Figure 21: Significant wave height, Oct 1990, Almagrundet

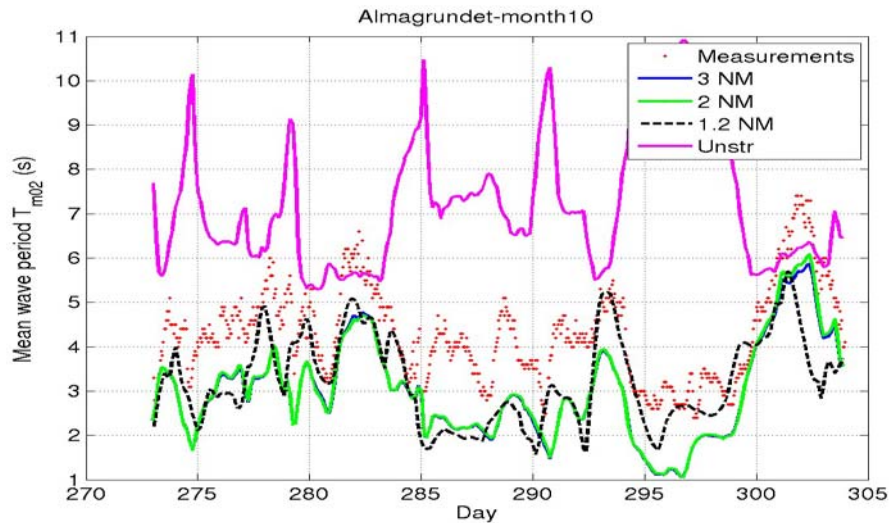


Figure 22: Mean zero crossing period, T_{m02} , Oct 1990, Almagrundet

To judge the quality of the data, scatter plots of model versus observed wave height and period are developed as in figures below. As the output from the SWAN model is every three hours and measured data are every one hour, we take the average of three consecutive measured data to match the corresponding third hour output from model. The blue line is the perfect fit to the model and observed values and the red dash line the symmetric slope (a least square fit to a linear function). Two statistical parameters are calculated: correlation coefficient and scatter index. Table 1 shows a summary of these parameters from the simulations with different computational grid types. Scatter index is defined as below;

$$SI = \frac{\text{standard deviation of errors}}{\text{average obs}} \times 100\%$$

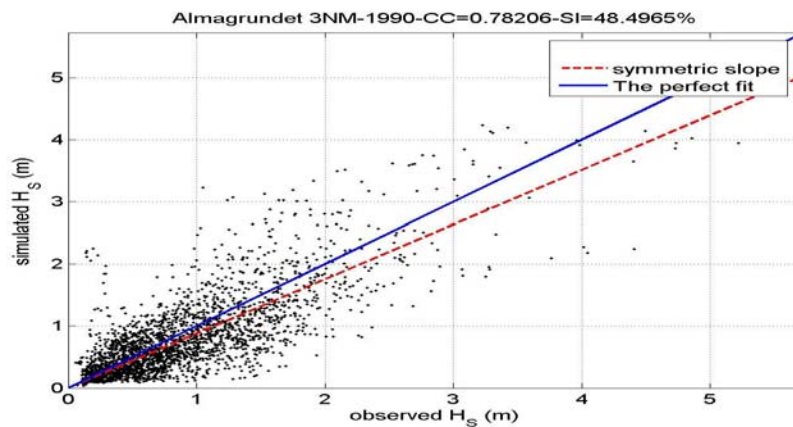


Figure 23: Scatter plot of 3 NM model versus observed wave height in 1990 at Almagrundet.

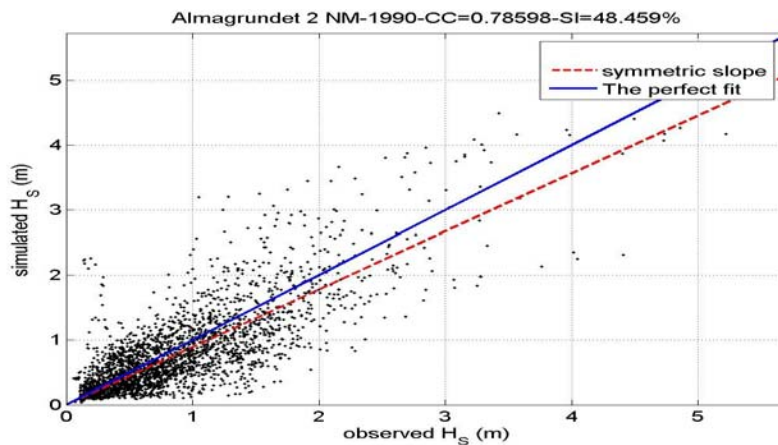


Figure 24: Scatter plot of 2 NM model versus observed wave height in 1990 at Almagrundet.

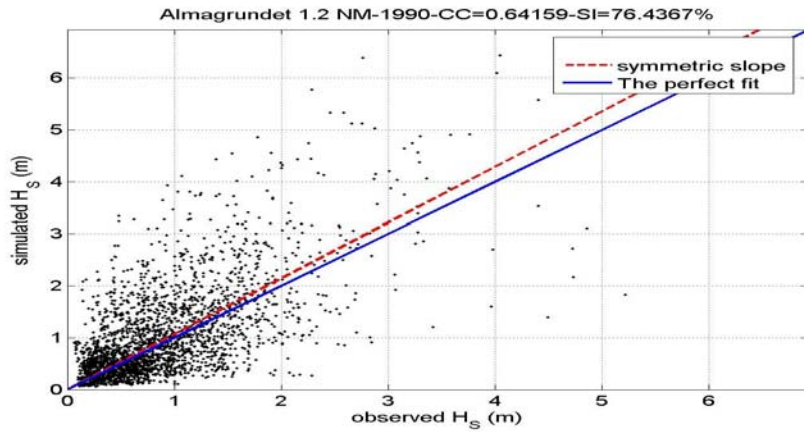


Figure 25: Scatter plot of 1.2 NM model versus observed wave height in 1990 at Almagrundet.

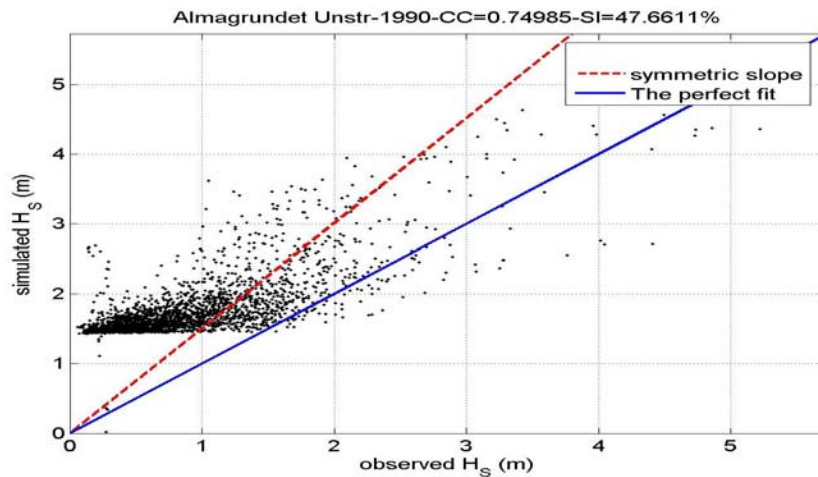


Figure 26: Scatter plot of unstructured model versus observed wave height in 1990 at Almagrundet.

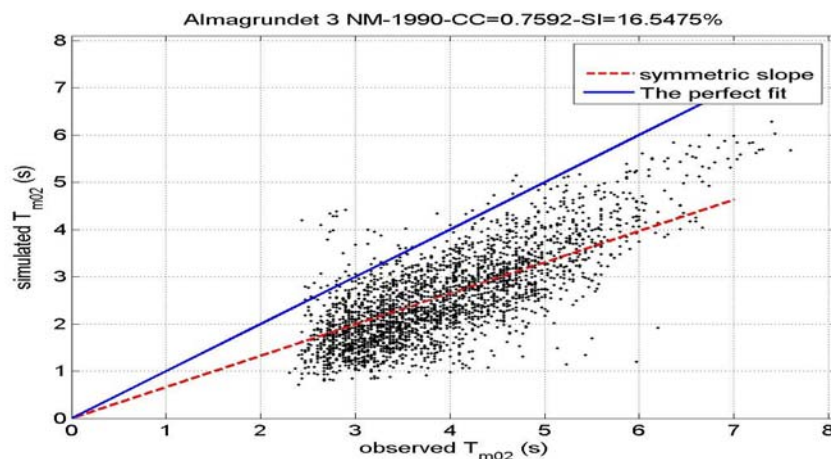


Figure 27: Scatter plot of 3 NM model versus observed mean wave period (T_{m02}) in 1990 at Almagrundet.

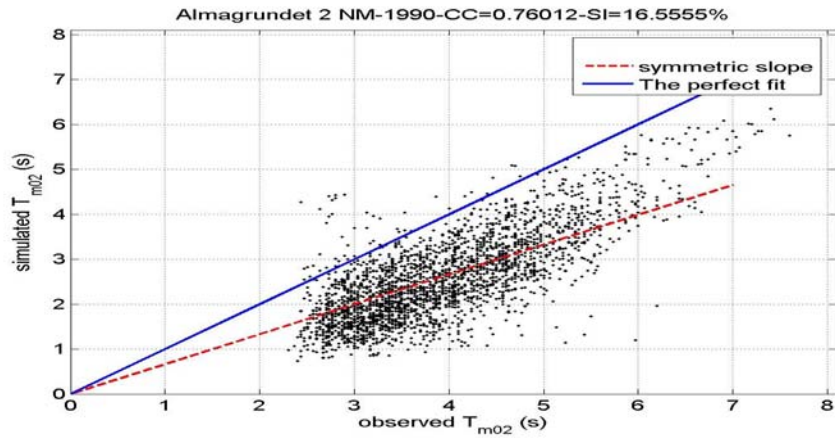


Figure 28: Scatter plot of 2 NM model versus observed mean wave period (T_{m02}) in 1990 at Almagrundet.

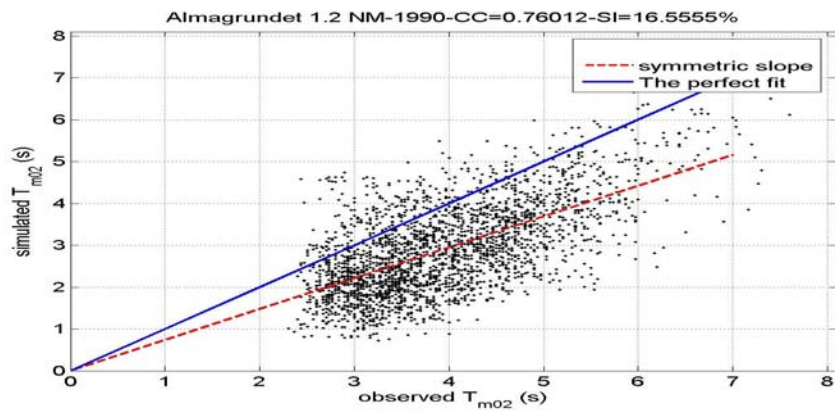


Figure 29: Scatter plot of 1.2 NM model versus observed mean wave period (T_{m02}) in 1990 at Almagrundet.

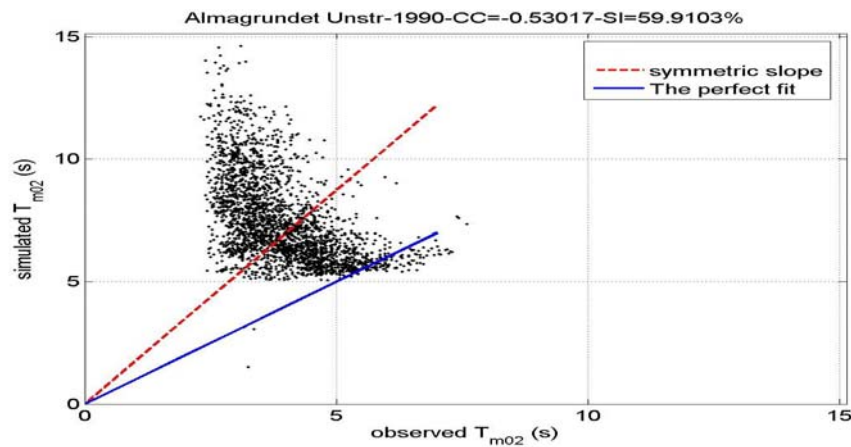


Figure 30: Scatter plot of unstructured model versus observed mean wave period (T_{m02}) in 1990 at Almagrundet.

Table 1: Statistical parameters from modeled and observed values during one year 1990, CC: correlation coefficient, SI: scatter index

1990	Significant wave height		Mean wave period	
	CC	SI	CC	SI
Almagrundet	0.78	48.49%	0.75	16.54%
3 Nm	0.78	48.45%	0.76	16.55%
2 Nm	0.64	76.43%	0.76	16.55%
1.2 Nm	0.74	47.66%	-0.53	59.9%

Smaller scatter index and correlation coefficient closer to 1.0 indicates better matching of simulation results with observations. The run with unstructured computational grids gives unacceptable results especially for mean wave period. The simulations with 2 and 3 NM resolution give similarly good results, but then the data quality drops when the resolution gets finer to 1.2 NM. By considering the computational efficiency, grids with 3×3 NM resolutions are the optimum choice among the scenarios.

4.2 Validation

The structured computational grid with the resolution of 3×3 nautical miles turned out to be the best option according to the results from first run. Now in order to validate this choice, a run with 3 NM structured computational grid and duration of one year in 1999, covering the whole region of Baltic Sea, Skagerack and Kattegatt, has been done. The wave measurement devices which were operating in this period are Almagrundet, Fladen, Ölands Södra Grund and Trubaduren. The scatter plots of model versus observations are presented for significant wave height and mean wave period (T_{m02}) in the figures below. The blue line shows the perfect fit to the model and observed values and the red dash line shows the symmetric slope (when the red line is below the blue the model underestimates the observed values). The summary of their statistical parameters are presented in Table 2.

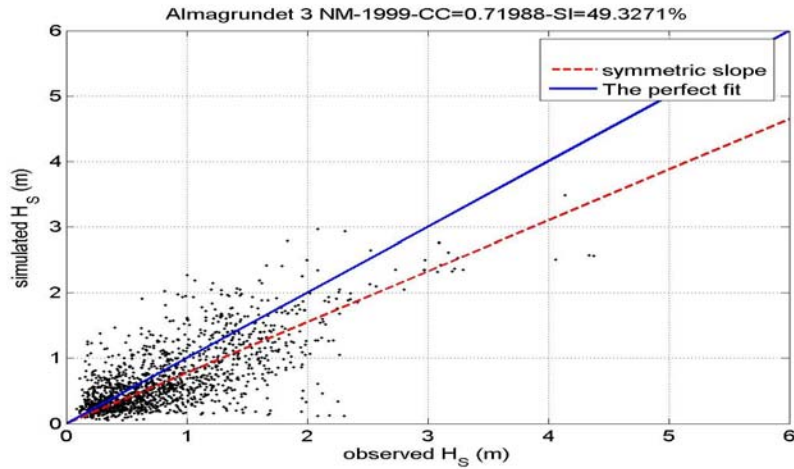


Figure 31: Scatter plot of model versus observed wave height based on data of 1999, January to December at Almagrundet.

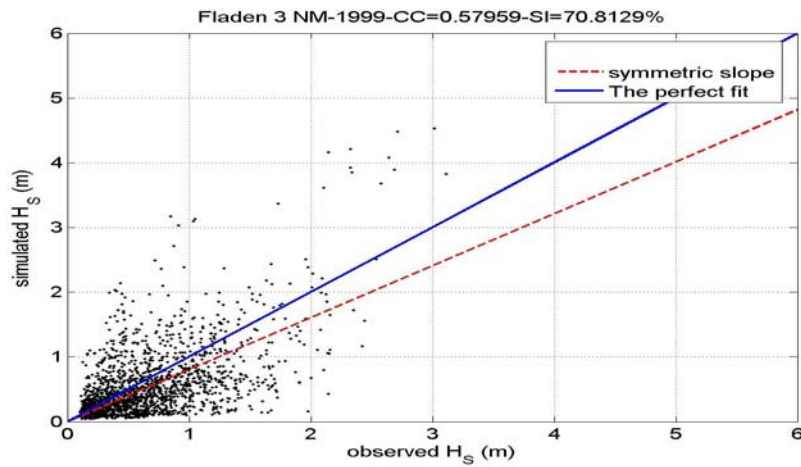


Figure 32: Scatter plot of model versus observed wave height based on data of 1999, January to December at Fladen.

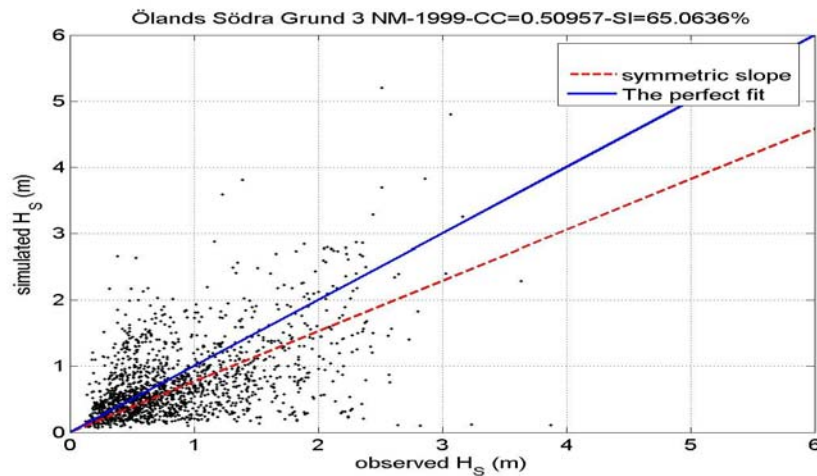


Figure 33: Scatter plot of model versus observed wave height based on data of 1999, January to December at Ölands Södra Grund.

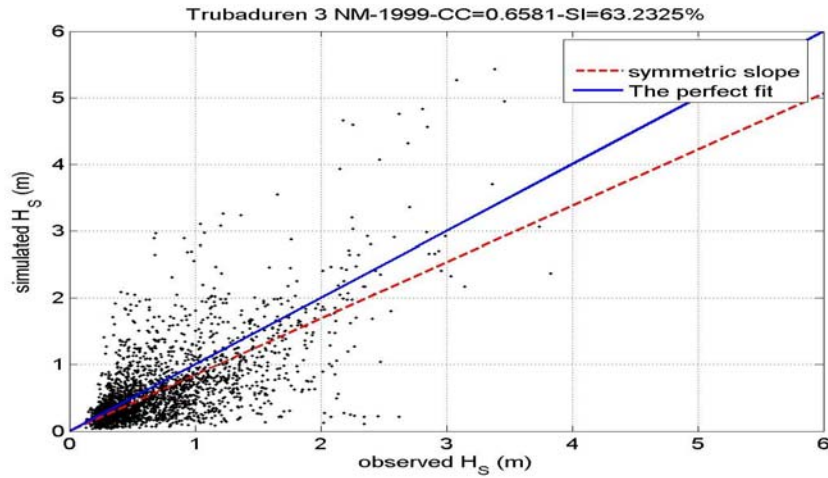


Figure 34: Scatter plot of model versus observed wave height based on data of 1999, January to December at Trubaduren.

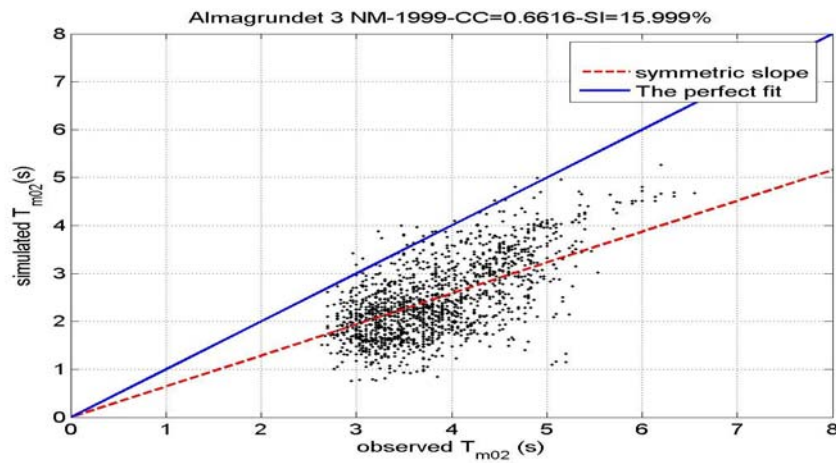


Figure 35: Scatter plot of model versus observed mean wave period (T_{m02}) based on data of 1999, January to December at Almagrundet.

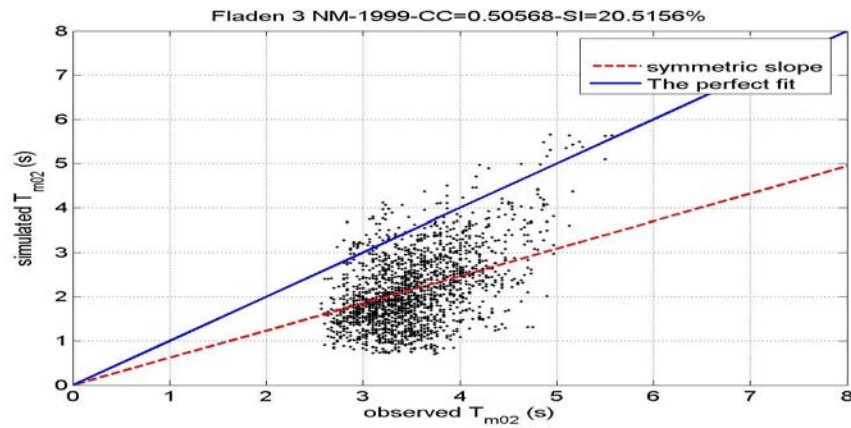


Figure 36: Scatter plot of model versus observed mean wave period (T_{m02}) based on data of 1999, January to December at Fladen.

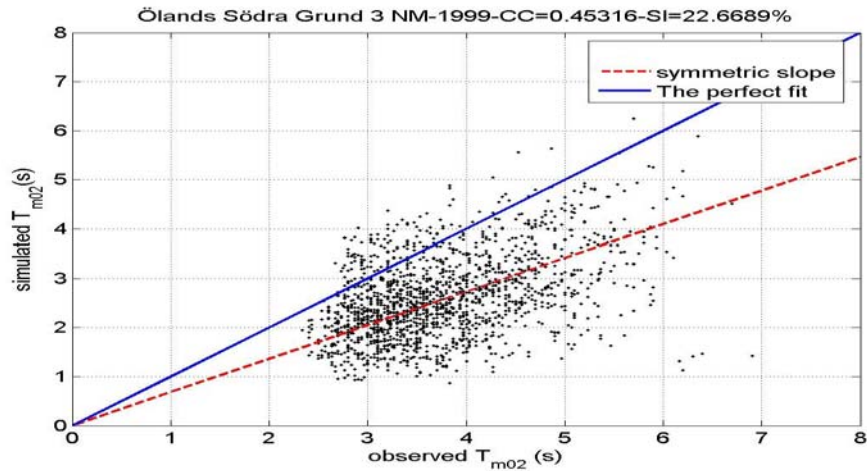


Figure 37: Scatter plot of model versus observed mean wave period (T_{m02}) based on data of 1999, January to December at Ölands Södra Grund.

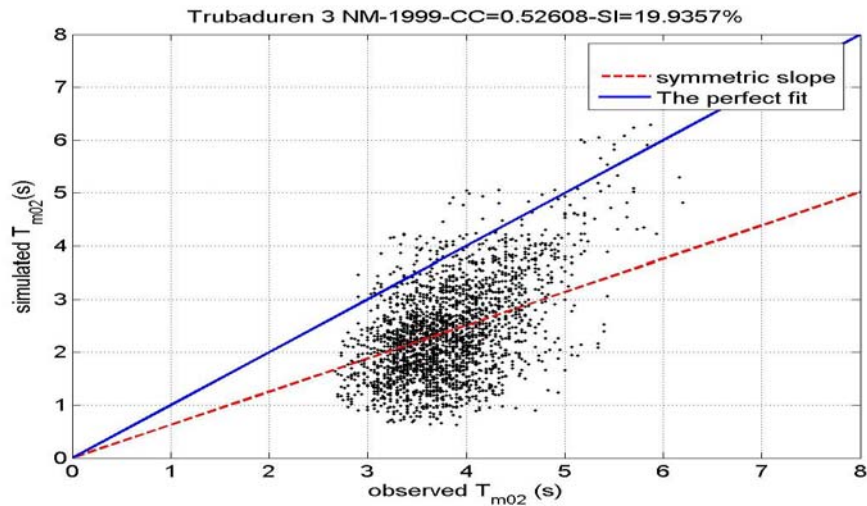


Figure 38: Scatter plot of model versus observed mean wave period (T_{m02}) based on data of 1999, January to December at Trubaduren.

Table 2: Statistical parameters from modeled and observed values during one year 1999, CC: correlation coefficient, SI: scatter index

1999	Significant wave height		Mean wave period	
	CC	SI	CC	SI
3 NM				
Almagrundet	0.72	49.33%	0.66	16 %
Fladen	0.58	70.81%	0.5	20.51%
OlandsSG	0.51	65 %	0.45	22.66%
Trubaduren	0.66	63.23%	0.52	20 %

4.3 Simulations time and data capacity

The time it takes for a simulation to run and the capacity required for data storage are important factors from the practical point of view. Unreasonably long runs and too large data to be stored will affect the efficiency of creating a data base. Table x shows the computation times at the calibration runs in the small nested region.

Table 3: Computation times for different grids at small nested region

Computational grid resolutions	Simulation times for 1990 (hours)
3 NM	7.6
2 NM	16.2
1.2 NM	42.4
Unstructured	65

The simulation covering the North Sea with grid resolution of 12×12 NM took 110 minutes, using OpenMP parallel processing communication tool and 1 node (8 kernels). The simulation covering the Baltic Sea, Kattegat and Skagerrak having the structured computational grid with the resolution of 3×3 NM, running for the year 1999, took about 42 hours on two nodes (16 kernels) using MPI libraries. The size of the results from this run, after removing the dry points, is about 1.3 Giga bytes.

In Table 4 the simulations covering the whole region are compared regarding their times. The first row with 6×6 NM computational and bathymetric grids represents the simulation of the old database. The second row has the same computational grid resolution but using the resolved bathymetric database. This was the coarse run containing information for the nested simulations at calibration runs. Producing boundary condition data for the nested simulations might be the main reason for such relatively long simulation time. The last row is the final validation run with both resolved computational and bathymetric grids.

Table 4: Computation times for simulations with different computational and bathymetric grids covering the Baltic Sea, Kattegat and Skagerrak

Computational grid resolution	Bathymetric data resolution	Year	Simulation time (hours)
6×6 NM	6×6 NM	1990	4
6×6 NM	1×1.6 NM	1990	25.6
3×3 NM	1×1.6 NM	1999	42

4.4 Comparison with previous simulation in 2008

In 2008 a run where the computational and bathymetric grids had the resolution of 6×6 NM was done. In this project the same input for wind and ice coverage is used but considering the shallow water physics and implementing resolved structured computational grids of 3×3 NM and bathymetric data with resolution of 1.0×1.6 NM. The year 1999 is chosen to compare the statistical parameters of the results at measurement stations, see Table 3.

The 99th percentiles significant wave heights for 1999 has been plotted from both databases (see Figures 26 and 27). Generally there is not any significant difference in the data quality but the new simulation has included much more details at coastlines which is an advantage to the previous one.

Table 5 statistical parameters from modeled and observed values during one year 1999, from the coarse 12x12 NM run in 2008 and the 3x3 NM run in this project, CC: correlation coefficient, SI: scatter index

	1999	Significant wave height		Mean wave period	
		CC	SI	CC	SI
Almagrundet	3 NM, 2010	0.72	49.33%	0.66	16 %
	6 NM, 2008	0.69	53.51%	0.63	17.21%
Fladen	3 NM, 2010	0.58	70.81%	0.5	20.51%
	6 NM, 2008	0.57	73.19%	0.5	21%
ÖlandsSG	3 NM, 2010	0.51	65 %	0.45	22.66%
	6 NM, 2008	0.49	66.65%	0.43	23.22%
Trubaduren	3 NM, 2010	0.66	63.23%	0.52	20 %
	6 NM, 2008	0.65	62.39%	0.53	19.6%

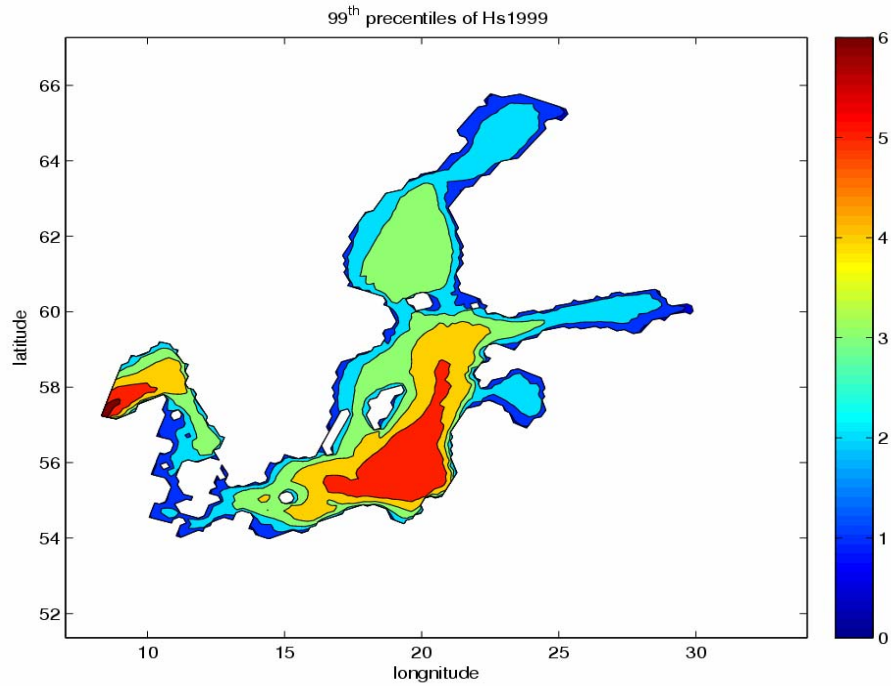


Figure 39: 99th percentiles of H_s 1999 at 6 NM grid resolution

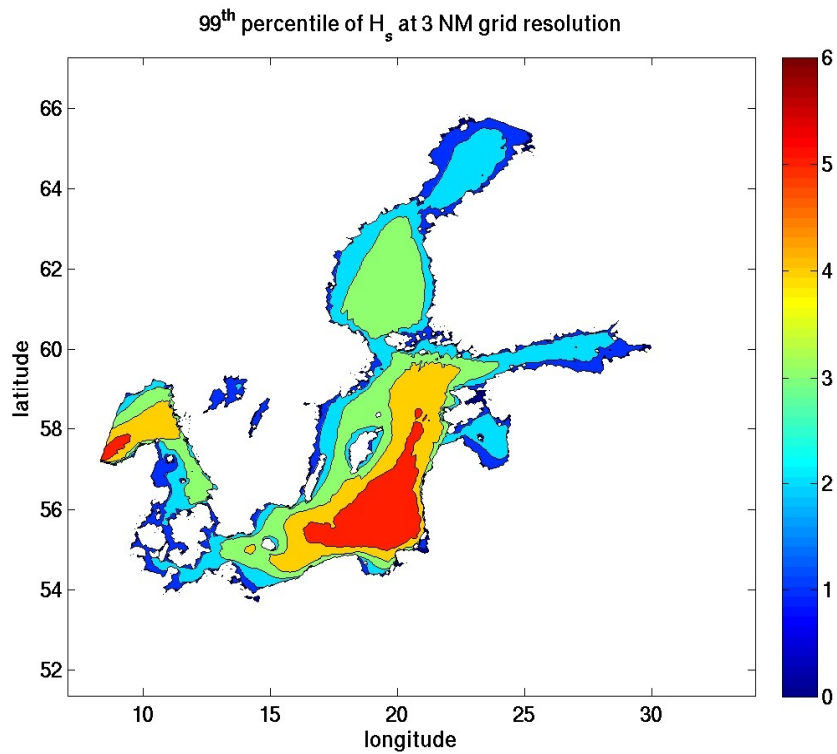


Figure 40: 99th percentile of H_s 1999 at 3 NM grid resolution

5 Discussion

According to the results, modified computational grid, better resolved bathymetric database and including the shallow water physics in the simulations have slightly improved the quality of the results. The effect of including shallow water physics into simulation could be better quantified if not all the measurement stations were located in offshore and deep areas. Using a refined bathymetric database has helped the simulation to model the irregularities of the coastal areas in much more detail. But in general the influence of the studied parameters in this work is much less than the effects of a modified wind database. [Broman and Kriezi (2008) and Howard et al. (2009)]

Applying unstructured grids, using TRIANGLE mesh generator, did not give any acceptable results. Before simulating the small nested region, several test runs have been done using triangular meshing and none of them gave satisfactory results. More investigations regarding this problem may be done in the future.

Refining the computational structured grids' resolution to 2 and 3 NM slightly improved the results as compared to the previous simulation with 6 NM grid resolution. The quality of the results drops by further refinement to the resolution of 1.2 NM. This could be interpreted as that there exists an optimum computational grid resolution relative to the bathymetric data and other inputs.

Comparing the results from simulations with 2 and 3 NM grid resolutions shows almost no difference. Considering the computational efficiency (time and data storage capacity) running the simulation with 3 NM resolutions is more efficient. Running the whole region for one year in 3 NM resolutions takes 42 hours and requires 1.3 GB memory for data storage. So for creating the 15 year hindcast, up to 630 hours processing and about 19.5 GB memory is required.

According to the results, a perfect fit between the simulation results and the observations has not been achieved. There are several factors behind this. Most importantly the RCA wind database, which provides atmospheric forcing for the model, doesn't have fully realistic and perfect data. Although Broman and Kriezi (2008) modified its underestimated wind speeds, it still cannot be considered as a fully realistic database. Furthermore, measurement devices provide data for every one hour, which is the average of a ten minute measurement, and the simulation has the wind input every third hour. Even by comparing the average from three consecutive measured values, still the compared values are not exactly corresponding to each other. Also there is the fact that measurement devices are not fully trustable, due to technical errors which might happen during their operation.

5.1 Improvements to previous database

- Slightly better correlation between simulation results and measurements.
- Irregularities at coastlines have been modelled with much more details. This means that more precise information will be available at coastal and shallow areas.
- The new bathymetric database contains the inland lakes. As the wind database covers the whole region, SWAN has simulated the lakes as well, but these results are not yet validated.
- By having better results at measurement stations it's likely to also have improved results at coastal areas.

5.2 Recommendations for further investigation and more development

In this work, it became clear that none of the parameters has as significant influence as the atmospheric input could have on the quality of the database in offshore areas. The primary option for further improvement of this database is to use a more realistic accurate wind database, such as the MESAN.

Use of structural computational grids, when refining to an appropriate resolution for having more detailed simulated coastlines, produces many unnecessarily fine computational cells out at the offshore regions. Unstructured (triangular) grids are one solution to this inefficiency. In this project, trying triangular meshes made by TRIANGLE faced many problems and the outcomes were not satisfactory. Exploring the TRIANGLE code, finding the reason of this problem, or trying other meshing codes may lead to a much more efficient simulation.

Evaluation of the simulation results has been done by comparing them to the measurements from few measurement stations. One way to evaluate the results in more points is using the satellite measurements recorded by altimeters. These databases cover the Baltic since about 20 years back. The waves' characteristics are estimated by evaluating the surface roughness which is measured by a radar system.

6 References

- Barstow, S., G. Mørk, L. Lønseth and J. P. Mathisen (2009): WorldWaves wave energy resource assessments from the deep ocean to the coast, European Wave and Tidal Energy Conference, Uppsala, Sweden.
- Broman, B. and E. Kriezi (2008): Past and future wave climate in the Baltic Sea produced by the SWAN model with forcing from the regional climate model RCA of the Rossby Centre. US/EU-Baltic International Symposium, May 27-29, 2008, Tallinn, Estonia.
- Broman, B., T. Hammarklint, K. Rannat, T. Soomere and A. Valdmann (2006): Trends and Extremes of wave fields in the north-eastern part of the Baltic Proper, *Oceanologia*, 48 (S), 2006, pp. 165-184.
- Dean, R.G. and R. A. Dalrymple (1991): *Water Wave Mechanics For Engineers And Scientists*, Allied Publishers, New Dehli, 2001.
- Dietrich, G. (1957): *General Oceanography, an Introduction*, John Wiley & Sons, USA, 1963.
- Hoque, M.A., S. M. Solomon and W. Perrie (2009): Nearshore waves in the Southern Beaufort Sea During severe arctic storms. Port and Ocean Engineering under Arctic Conditions, June 9-12, 2009, Luleå, Sweden.
- Howard, K., G. Zarillo, M. Splitt, S. Lazarus, S. Chiao, P. Santos, and D. Sharp (2009): The impact of atmospheric model resolution on a coupled wind/wave forecast system, 16th conference on Air-Sea Interaction, American Meteorological Society, January 2009, Seattle, Washington.
- Kantha, L.H. and C. A. Clayson (2000): Numerical Models of Oceans and Oceanic Processes.
- Komen, G.J. and K. Hasselmann (1984): On the existence of a fully developed wind-sea spectrum. *J. Phys. Oceanogr.* 14, 1271-1285.
- Miles, J.W. (1957): On the generation of surface waves by shear flows, *J. Fluid Mech.* 3: 185-204; 6: 568-582; 7: 469-478.
- Phillips, O.M. (1957): On the generation of waves by a turbulent wind. *J. Fluid Mech.*
- Rusu, E. (2009): Wave energy assessments in the Black Sea. *Journal of Marine Science and Technology*, Vol. 14, No. 3, September 2009, pp. 359-372.
- Shewchuk, J.R. (1996): *Triangle: Engineering a 2D Quality Mesh Generator and Delaunay Triangulator*, Applied Computational Geometry: Towards Geometric Engineering (Ming C. Lin and Dinesh Manocha, editors), volume 1148 of Lecture Notes in Computer Science, Springer-Verlag, Berlin, May 1996, pp. 203-222.
- Silvester, R. (1974): *Coastal Engineering, I, Generation, propagation and influence of waves*, Elsevier, Amsterdam, Netherlands.
- Snyder, R.L. and C. S. Cox (1996): A field study of the wind generation of the ocean waves. *J. Marine Res.*, 24(2), 141-178.

- Snyder, R. L., F. W. Dobson, J. A. Elliott and R. B. Long (1981): Array measurements of atmospheric pressure fluctuations above surface gravity waves. *J. Fluid Mech.*, 102, 1-59.
- The SWAN team (2008): *SWAN Cycle III version 40.72 user manual*, Delft University of Technology, Delft, Netherlands.
- Tuomi, L. and A. Sarkanen (2008): Wave forecasts for the Baltic Sea using ECMWF wind fields as forcing data, US/EU-Baltic International Symposium, May 27-29, 2008, Tallinn, Estonia.
- Wamsley, V. (2009): Interaction of hurricanes and natural coastal features, implications for storm damage reduction, Water resources engineering, faculty of Engineering, Lund University, Sweden.
- Wiegel, R.L. (1964): *Oceanographical Engineering*, Prentice-Hall, Englewood Cliffs, N.J. USA.
- World Meteorological Organization (1998): *Guide to wave analysis and forecasting*, WMO, No. 702, Geneva, Switzerland.
- Young, I.R. (1999): *Wind Generated Ocean Waves*, Elsevier, Amsterdam, Netherlands.